POLITECNICO DI TORINO

I Facolta di Ingegneria

Master Universitario di II Livello

TESI DI LAUREA

GROUND REACTION CURVE OF REINFORCED TUNNEL USING A NEW ELASTO-PLASTIC MODEL

A POST GRADUATE THESIS SUBMITTED TO

THE LAND, ENVIRONMENT AND GEO-ENGINEERING DEPARTMENT

OF

THE TECHNICAL UNIVERSITY OF TURIN

(Politecnico di Torino)

Candidate: Ing. Reza Rangsaz Osgoui

Academic Tutor: Prof. Ing. Pierpaolo Oreste

Company Tutor: Prof. Ing. Daniele Peila

Torino- Italia

NOVEMBER 2006

ABSTRACT

GROUND REACTION CURVE (GRC) OF REINFORCED TUNNEL USING A NEW ELASTO-PLASTIC MODEL

Reza Rangsaz Osgoui

Post Graduate in Tunnelling and Tunnel Boring Machines, Department of

Land, Environment and Geo-engineering

Politecnico di Torino in partnership with COREP

Academic Tutor: Prof. Ing. Pierpaolo Oreste

Company Tutor: Prof. Ing. Daniele Peila

November 2006, 79 Pages

Incredible increase in applications of NATM and open-mode TBM tunnelling; especially in great depth and poor quality rock mass entails maintaining rock mass behind and ahead of the tunnel face. Rock reinforcing techniques has been found to be one of the most practical means to stabilize the tunnel by improving rock mass. Accompanied with injection, grouted rock bolting can be considered as a ground improvement option, whereby the shear strength of the rock mass can be raised to such an extent that a considerable decrease in plastic zone and convergence of tunnel are achieved. Grouted rock bolting is a means capable of modifying the convergence-confinement curve and modifying the value of the radial displacement at the moment of the installing the final lining. Hence, this Post-Graduate thesis is intended to provide an alternative solution to investigate the effect of the radial passive rock bolting on mechanical behaviour of rock mass around the tunnel.

This theoretical study presents a rigorous, elasto-plastic solution for the axi-symmetrical problem of an unsupported circular tunnel and adopts a proper interaction mechanism between the ground and the grouted bolts in generalized Hoek & Brown material. The essential aim of this solution is intended to predict the stresses and displacements fields and extent of plastic zone around a deep circular tunnel subject to a hydrostatic stress field. In this analysis the rock mass obeys the latest Hoek & Brown yield criterion (version 2002) and a non-associated flow rule is used. For the elastic–brittle–plastic analysis of circular openings in an

infinite Hoek–Brown medium, the existing analytical solutions were found to be very complex and none of them has been developed based on latest Hoek & Brown yields criterion. Although most of the existing elasto-plastic solutions for tunnel problems in Hoek & Brown media consider an intact rock (i.e., $a = 0.5$), the proposed approach supposes $a \geq 0.5$ for rock mass. In addition, this solution is based on the assumption that after the intact strength of the rock is exceeded, the material loses its strength, as dictated by a 'strength loss' parameter (S). The solution allows a representation of the Ground Reaction Curve for tunnels, which is used in convergence-confinement method. The proposed model is not valid if a pronounced discontinuity intersects the opening or when anisotropic conditions prevails but it assumes that the joint system present in the rock mass has no preferred orientation so that the medium can be considered to behave as an isotropic continuum. Illustrative applications of the derived elasto-plastic solutions are also described and the results are compared with those obtained with numerical techniques. The present elasto-plastic solution was validated by using the finite difference method in the form of both quarter and axi-symmetric model. The proposed analytical solution is capable of predicting the ultimate tunnel convergence (at least two tunnel diameters behind the face), where three-dimensional face effects are ignored. An axi-symmetrical numerical modelling has proved the ability of the analytical model in this respect. It is assumed that the excavated tunnel face is immediately supported by fully grouted bolts, such that the time-dependent behaviour and loosening can be neglected.

In case of reinforced tunnel by grouted bolts, the proposed model provides an alternative method based on convergence control approach. It considers the influence of bolt/ground interaction, tunnel geometry and the pattern of bolts on plastic zone and the tunnel convergence. The shear stress distribution along the fully grouted bolts was chosen (semi-empirical) to satisfy equilibrium of the bolt relative to the surrounding ground. The concept of an equivalent plastic zone was introduced to describe the extent of yielding around a circular tunnel, reinforced with fully grouted bolts. Three stages (categories) of yield propagation have been defined and analyzed with respect to the relative location of the plastic zone boundary in contrast to the neutral point of zero shear stress on the bolt. A friction factor, λ, has been introduced as a characteristic parameter for the bolt-ground composite interaction. The effect of bolt density parameter (β), which reflects the relative density of bolts with respect to the tunnel perimeter and takes into consideration the shear stresses opposing the rock mass displacements near the tunnel wall, on strength parameters of rock mass and the extent of plastic zone reveals the role of bolt spacing and bolt / grout frictional interaction in design, which in turn provides a means of selecting an optimum reinforcement pattern. At the end, the Ground Reaction Curve in the presence of rock bolting based on the proposed elasto-plastic solution will readily obtained.

Keywords: Elasto-plastic solution, Reinforcement design, Grouted bolt, Ground Reaction Curve, Tunnelling.

To My Family

ACKNOWLEDGEMENTS

TABLE OF CONTENTS

NOMENCLATURE

r_i = tunnel radius

r = distance from tunnel center to point of interest

r_e = radius of plastic (broken, yielding) zone

r_e^* = radius of Equivalent Plastic Zone (EPZ)

P_o = far field stress

P_i = support pressure

σ_r = radial stress

σ_θ = tangential stress

σ_{re} = radial stress at elastic-plastic interface

σ_1 = maximum principal stress

σ_3 = minimum principal stress

σ_{ci} = uniaxial compressive strength of intact rock

σ'_{ci} = residual compressive strength of intact rock

S = post-peak strength reduction factor

C_b = bolt capacity

RMR = Rock Mass Rating of Bieniawski

Q = Rock Quality Index of Barton

GSI = Geological Strength Index

D = disturbance factor

m_b = strength constant of Hoek & Brown Failure criterion

s = strength constant of Hoek & Brown Failure criterion

a = strength constant of Hoek & Brown Failure criterion

m'_b = residual strength constant of Hoek & Brown Failure criterion

s' = residual strength constant of Hoek & Brown Failure criterion

a' = residual strength constant of Hoek & Brown Failure criterion

m_b^* = equivalent strength constant of Hoek & Brown Failure criterion

σ_{ci}^* = equivalent strength of intact rock

s^* = equivalent strength constant of Hoek & Brown Failure criterion

c = cohesion of rock mass

c^* = equivalent cohesion of rock mass

ψ = dilatancy angle of rock

ϕ = friction angle of rock

N_ψ = dilation coefficient

ν = poisson's ratio

E = Young's modulus

G = shear modulud

K = bulk modulus

ε_r^e = elastic radial strain increment

ε_r^p = plastic radial strain increment

ε_r^t = total radial strain

ε_θ^e = elastic tangential strain increment

ε_θ^p = plastic tangential strain increment

ε_θ^t = total tangential strain

L_b = bolt length

d = bolt diameter

τ_z = shear stress distribution along a grouted bolt

σ_z = axial stress distribution along the bolt

S_T = transversal (circumferential) bolt spacing

S_L = longitudinal bolt spacing

ρ = radius of the neutral point of the bolt

λ = friction factor for bolt/ grout interface

β = bolt density parameter

u_{ri} = displacement (convergence) of unsupported tunnel

u_{ri}^* = displacement (convergence) of reinforced tunnel

u_{ri}^*/u_{ri} = normalized convergence ratio

u_e = elastic tunnel displacement (convergence)

BE = bolt effectiveness

INTRODUCTION

These days, the applicability of the grouted rock bolts has been successfully put into practice in conventional tunnelling. Most of tunnelling methods such as New Austrian Tunnelling Method (NATM) adopt a practical way to combine grouted bolts with steel sets, shotcrete and weld-mesh to provide a most efficient and economical support system that can be installed soon after excavation. However, the use of the grouted rock-bolts has also been attracted plausible acceptance in mechanized tunnelling. Presently, transversely and longitudinally installed grouted bolts in open-type TBMs and shielded-TBMs have being broadly practiced.

The analytical solution presented in this thesis constitutes an extension of the application of elasto-plasticity to the design of grouted rock bolts. It provides an alternative method based on a convergence control approach. The proposed analytical model considers the influence of bolt/ground interaction, opening geometry and the pattern of bolts on yielding zone and the tunnel convergence. The ground reaction curve of unsupported and reinforced tunnel can be ultimately depicted to find out the how much the bolting action decreases and controls the tunnel convergence.

The thesis has been organized in two main chapters:

Chapter 1 deals with the development of a rigorous, elasto-plastic solution for the axi-symmetrical problem of an unsupported circular tunnel in generalized Hoek & Brown material (Version 2002). The stresses, displacements, and yielding (plastic) zone around the tunnel are determined based on new mathematical formulations. In addition, the validity of the proposed elasto-plastic model has been verified by numerical modelling as outlined in this chapter.

The Equivalent Strength Parameter concept in combination with elasto-plastic solution is a framework in the reinforced tunnel analysis as will be discussed in the Chapter 2. The proposed analytical solution provides a practical means to design of the grouted bolts based on convergence control approach. It considers the influence of bolt/ground interaction, tunnel geometry and the pattern of bolts on plastic zone and the tunnel convergence. The introduction of the equivalent plastic zone associated with bolted tunnel is explained and examined in terms of the different magnitude of bolt densities and lengths.

CHAPTER 1

1   DEVELOPMENT OF A NEW ANALYTICAL ELASTO-PLASTIC SOLUTION FOR UNSUPPORTED TUNNEL

1.1   Introduction

An ealsto-plastic solution makes it possible to determine the stresses, the displacements, and the radius of the plastic zone around the tunnel. For the assumption of the isotropy in field stress, circular shape of tunnel, homogeneity in rock mass, and axi-symmetrical plane strain condition, several approaches have been developed over the past 30 years (Ladanyi 1974, Florence & Schwer 1978, Hoek & Brown 1980, Brown et al. 1983, John et al. 1984, Deournay & John 1988, Senseny *et al.* 1989, Indraratna & Kaiser 1990 , Pan & Chen 1990, Panet 1993, Duncan Fama 1993, Cundall et al. 2003,Wang 1996 , Ogawa & Lo 1987, Carranza-Torres & Fairhurst 1999, Carranza-Torres 2004, Sharan 2003, 2005, Park & Kim 2006).

The assumption of homogeneity, isotropy and linear elasticity before yielding occurs are made to simplify the analysis. The application of Airy's stress functions and Hooke's law to determine the stress and strain fields constitutes the fundamentals of the elastic theory (Timoshenko & Goodier, 1970). Since tunnels are much longer than their diameter, it is reasonable to assume that the plane strain condition (longitudinal strain is neglected) prevails ultimately. The conditions at the face differ significantly and, hence, three dimensional effects should be considered. For the following, it is assumed that this transition does not affect the final bolt behaviour.

The extent of yielding (plastic zone radius) is dependent on the material properties of the rock mass, the in-situ field stress and the tunnel radius (tunnel span). Yielding may be followed by rupture of the wall if uncontrollable deformations occur in weak ground. It is the objective of radial rock-bolting to minimize large displacements in order to maintain a coherent load bearing ring around the tunnel. The installation of bolts effectively improves the apparent material properties of the rock mass thereby reducing strains and displacements.

The analysis presented in this chapter is a rigorous elasto-plastic solution to assess the stresses and displacements of an unsupported tunnel and to investigate

the influence of fully grouted rock-bolts on the rock mass behaviour around the tunnel. The following major assumptions have been made in this analysis:

I.   Deep circular tunnel in hydrostatic stress fields (k=1)

II. Homogeneous, isotropic material with time-independent properties

III. Elastic-brittle-plastic strength model (Figure 1-4) with non-linear Hoek & Brown yield criterion (version 2002, Hoek *et al.* 2002). Plastic deformations follow a flow rule with constant rate of dilation

IV. Deformation pattern near the tunnel is properly described by plane strain condition. Three dimensional effects at tunnel face are neglected.

V.   Shear stress distribution along the fully grouted bolts is assumed by the model illustrated in Figure 2-1. The influence of the relatively thin grout annulus on rock mass deformation has been ignored.

VI. Axi-symmetric bolt pattern around the excavation consists of identical bolts with equal spacing along the tunnel axis and around the circumference. The tangential bolt spacing around the opening is defined by the product of the tunnel radius and the angle between two adjacent bolts (i.e $S_t = r_i.\theta$) as shown in Figure 2-2.

The followings are the distinguishable steps of elasto-plasticity analysis that will be determined in the proposed solution:

I.   Constitutive model of material behaviour

II.   Lame's solution for determination of the stresses in the elastic zone

III. Stress in plastic (yielding, overstressed, broken, undisturbed) zone

IV.   Stress at the interface of plastic and elastic zones

V.   Radius of plastic zone

VI.   Strains and displacements in the elastic zone

VII. Strains and displacements in the plastic zone

VIII. Radial displacement or tunnel convergence (closure)

1.2   Definition of the problem

The problem is defined in Figure 1-1. Consider a circular opening being excavated in an infinite medium subjected to isotropic initial stress, P_o. The excavation removes the boundary stresses around the circumference of the opening, and the process may be simulated by gradually reducing the internal (support) pressure, P_i. As P_i is reduced, a plastic zone is formed when the material is

overstressed, and the radial displacement, u_r, occurs. It is required to compute the stresses and displacements around the tunnel, when plane strain condition along the axis of the tunnel is reached.
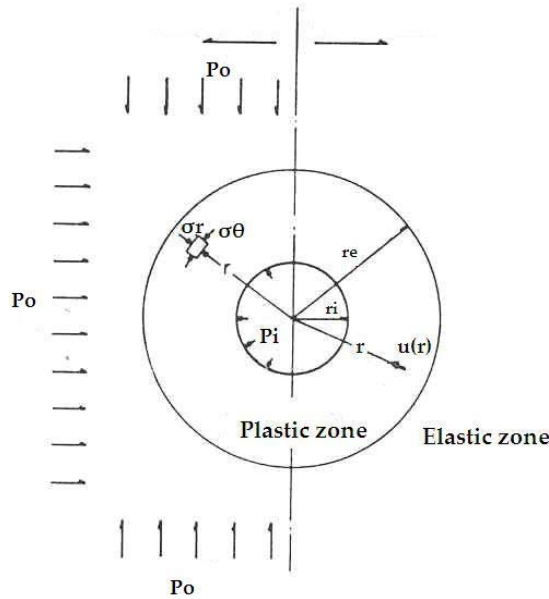
Figure 1-1 Definition of the model

1.3   Method of solution

For a solution of the elasto-plastic problem, the equation of equilibrium, compatibility condition, stress- elastic strain relationship, yield criteria, plastic potential, and a flow rule are required. The stresses and displacements in the elastic region may be readily determined by observing the continuity of radial stresses and displacements at the elastic-plastic interface. The solution within the plastic region will depend on the assumption of (a) the yield criterion, (b) the use of associated or non-associated flow rule, and (c) the dilatancy angle ψ.

Under the axi-symmetric plane strain condition, the strains and the displacements are expressed as

$$u_r = u_r(r), u_\theta = 0, u_z = 0 \tag{1-1}$$

$$\varepsilon_r = \frac{\partial}{\partial r} u_r, \varepsilon_\theta = \frac{u_r}{r}, \varepsilon_z = 0 \tag{1-2}$$

where the subscripts *r, θ,* and *z* denote respectively radial, tangential, and longitudinal (axial) directions. The compatibility condition is given by:

$$\frac{\partial}{\partial r}(r\varepsilon_\theta) = \varepsilon_r \quad \text{or} \quad \frac{\partial \varepsilon_\theta}{\partial r} + \frac{\varepsilon_\theta - \varepsilon_r}{r} = 0 \tag{1-3}$$

or in differential equation form:

$$\frac{d\varepsilon_\theta^t}{dr} + \frac{\varepsilon_\theta^t - \varepsilon_r^t}{r} = 0$$

For small deformation and infinitesimal strains, the total strains are divided into the elastic and plastic components

$$\varepsilon_{ij} = \varepsilon_{ij}^e + \varepsilon_{ij}^p \tag{1-4}$$

where the superscripts and *e* and *p* denote elastic and plastic components, respectively. Furthermore, the elastic strain component may be divided into the deviatoric and volumetric components (Timoshenko & Goodier, 1970) as

$$\varepsilon_{ij}^e = \varepsilon_{ij}^e + v^e \delta_{ij} \tag{1-5}$$

where ε_{ij}^e = elastic deviatoric strain component; v^e = elastic volumetric component $(\frac{1}{3}\varepsilon_{kk}^e)$ and

δ_{ij} =Kronecker's delta $\delta_{ij} = 1, (i = j) and \delta_{ij} = 0, (i \neq j) where (i, j = 1,2,3 or \theta, r, z)$.

Similarly, the stress component σ_{ij} is divided into the deviatoric and volumetric components:

$$\sigma_{ij} = \sigma_{ij}' + \sigma_o \delta_{ij} \tag{1-6}$$

where σ_{ij}' = deviatoric stress component, σ_o = volumetric stress component $(\frac{1}{3}\sigma_{kk})$, and the summation convention is implied by the repeated dummy indices.

The constitutive equations relating the deviatoric and volumetric components of stresses and elastic strains are therefore given by:

4

$$\varepsilon_{ij}^{e} = \frac{1+\nu}{E}\sigma_{ij}' \tag{1-7}$$

$$v^{e} = \frac{1-2\nu}{E}\sigma_{o} \tag{1-8}$$

where E is Elasticity or Young's modulus and ν is the Poisson's ratio.

The flow rule of plasticity relating the plastic strain increment $\dot{\varepsilon}_{ij}^{p}$ and the plastic potential Q is given by:

$$\dot{\varepsilon}_{ij}^{p} = \lambda\frac{\partial Q}{\partial\sigma_{ij}} \tag{1-9}$$

The above elasto-plastic stress- strain and stress-strain increment relationships are generally used, and are listed for completeness. The choice of yield criteria and plastic potential will be discussed in the following parts.

1.4   Yield criterion

Yield initiation is assumed to occur following a non-linear Hoek & Brown failure criterion. In this elasto-plastic solution the latest version of the Hoek & Brown yield criterion introduced in 2002 (Hoek *et al.* 2002) has been chosen to be the main constitutive model for behaviour of the rock mass.

The Hoek-Brown yield criterion for intact rock defines the combination of major and minor principal stresses (σ_1 and σ_3) at failure to be as:

$$\sigma_1 = \sigma_3 + \sigma_{ci}\left(m_i\,\frac{\sigma_3}{\sigma_{ci}}+1\right)^{\frac{1}{2}} \tag{1-10}$$

where σ_{ci} is the unconfined compressive strength of the rock and the coefficient m_i is a parameter that depends on the type of rock (normally $5 \leq m_i \leq 40$). Both parameters, σ_{ci} and m_i , can be determined from regression analysis of triaxial test results (Hoek & Brown 1980; Hoek *et al.* 1995).

The Hoek-Brown yield criterion was later extended to define the shear strength of rock masses. This form of the yield criterion, which is normally referred

to as the generalized Hoek-Brown yield criterion in terms of peak strength, is (Hoek, 1994 and Hoek & Brown, 1997):

$$\sigma_1 = \sigma_3 + \sigma_{ci}\left(m_b \frac{\sigma_3}{\sigma_{ci}} + s \right)^a \tag{1-11}$$

The coefficients m_b, s and a in Equations 1-10 and 1-11 are semi-empirical parameters that characterize the rock mass.

In practice, these parameters are associated with rock mass rating RMR and more recently the Geological Strength Index or GSI (Hoek, 1994, Hoek & Brown, 1997). This index lies in range 6 to 90 and can be quantified from charts based on the quality of the rock structure and the condition of the rock surfaces (Hoek & Brown 1997; Hoek, Marinos, & Benissi 1998).

In the latest update of the Hoek-Brown yield criterion, the relationship between the coefficients m_b, , s and a in Equation 1-11 and the GSI is as follows (Hoek *et al.* 2002):

$$m_b = m_i \exp\left(\frac{GSI - 100}{28 - 14D} \right) \tag{1-12}$$

$$s = \exp\left(\frac{GSI - 100}{9 - 3D} \right) \tag{1-13}$$

$$a = \frac{1}{2} + \frac{1}{6}\left(e^{-GSI/15} - e^{-20/3} \right) \tag{1-14}$$

Figure 1-2 depicts the Hoek & Brown yield criterion for different quality of rock masses (GSI= 100, 50, and 5).

In Equations 1-12 and 1-13, D is a factor that depends on the degree of disturbance to which the rock has been subjected to blast damage and stress relaxation. This factor varies between 0 and 1. Likewise, the generalized Hoek & Brown yield criterion in terms of the residual strength parameters can be defined as follow:

$$\sigma_1 = \sigma_3 + \sigma'_{ci}\left(m_b{}' \frac{\sigma_3}{\sigma'_{ci}} + s' \right)^{a'} \tag{1-15}$$

The primed constants stand for the residual (post-peak) values of the rock mass. The Figure 1-3 represents the definition of both peak and residual values of Hoek & Brown constants.
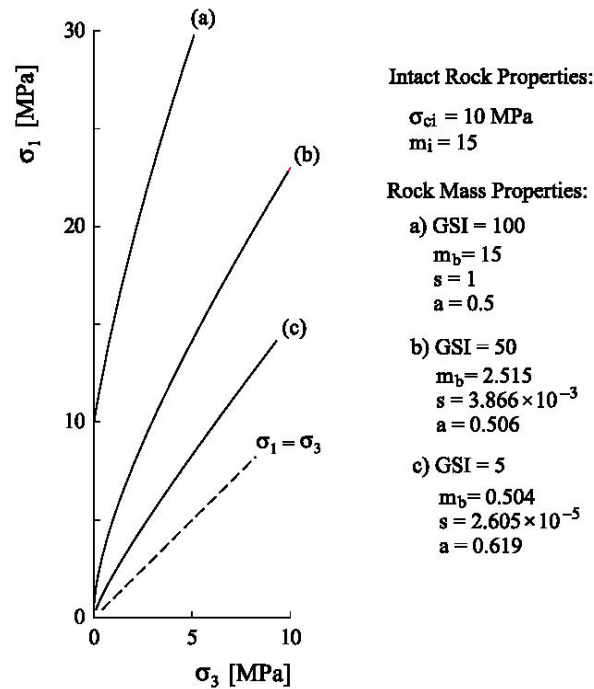
Figure 1-2 Hoek-Brown failure criterion for intact rock (curve a) and rock masses with decreasing values of GSI (curves b and c)

Post-peak (residual parameters) behaviour is characterized by the flow rule that governs the plastic deformations. In the perfectly plastic material model, there is no strength drop after peak; hence, yielding continues to occur at a constant peak stress level. However, a strain weakening behaviour is generally observed in most rocks where the post- failure behaviour is strain-dependent.

The elastic-brittle-plastic model is a simplification of the above described behaviour, and is characterized by an instantaneous strength drop at peak as shown in Figure 1-4. The Hoek & Brown failure criterion is still applicable although the post-peak strength is reduced.

It has been substantiated that the extension of the broken zone relies on the residual value of the intact rock strength (Hoek & Brown 1980, Brown *et al*. 1983, Indraratna & Kaiser, 1990a, Carranza-Torres, 2004). Hence, the effect of the compressive strength of rock material must be included in the form of the residual value because it loses its initial value due to stress relief or an increase in the strain. A stress reduction scale must, therefore, be considered as:

$$\sigma'_{ci} = S.\sigma_{ci} \qquad\qquad (1\text{-}16)$$

where S refers to the strength loss parameter quantifying the jump in strength from the intact condition to residual condition or a measure of the degree of strength loss occurring immediately after the peak strength is reached. The parameter S characterizes the brittleness of the rock material: ductile, softening, and brittle.
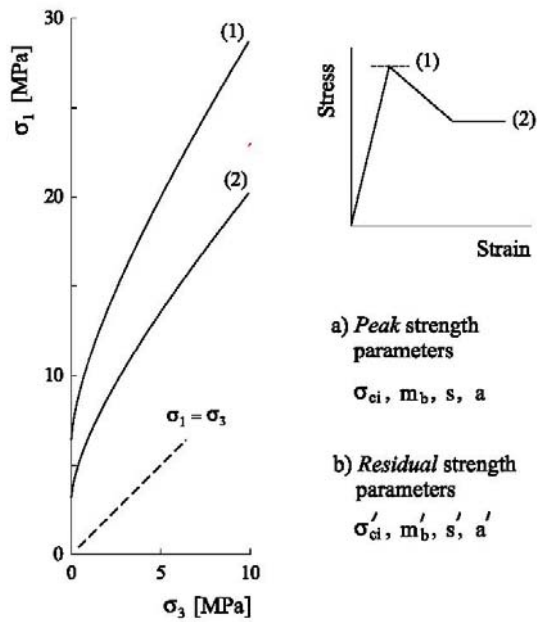
Figure 1-3 Peak and residual failure envelopes considered for the generalized Hoek-Brown failure criterion for the problem in Figure 1.1.
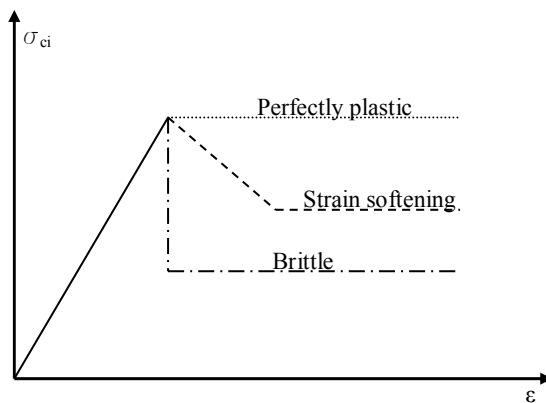
Figure 1-4 Different post-peak strength models of rocks

By definition, S will fall within the range $0<S<1$. Where $S= 1$ implies no loss of strength and the rock material is ductile, or perfectly plastic. By contrast, if $S=0$, the rock is brittle (elasto-brittle plastic) with the minimum possible value for the residual strength (i.e. $\sigma_1=\sigma_3$) as highlighted in the Figure 1-4.

1.5   Flow rule of plasticity and plastic potential

From the classical stress-strain curve standpoint, at the failure point and post –peak behaviour of a rock, it is important to determine the post-failure parameters of rock due to their applicability in the analysis of the deduced broken (yielded) zone as well as reinforced rock mass around the opening. The theory of plasticity is recognized to be a tool, whereby; post peak parameters of rock can be determined based on selective yield condition.

The flow rule of plasticity relating the plastic strain increment $\dot{\varepsilon}_{ij}^{p}$ and the plastic potential Q is, as shown before, given by (Hill, 1950):

$$\dot{\varepsilon}_{ij}^{p} = \lambda \frac{\partial Q}{\partial \sigma_{ij}} \tag{1-17}$$

where λ is a non-negative constant of proportionality which may vary throughout loading history. It is also necessary to be able to define the stress state at which yield will occur and plastic deformation will be initiated. For this purpose, a yield function $F(\sigma)$ is defined such that $F=0$ at yield. If $Q=F$, the flow law is said to be associated. In this case, the vectors of σ and ε^p are orthogonal; this is known as the normality condition.

The concept of associated plastic flow were developed for perfectly plastic and strain-hardening materials using yield functions such as those of Tresca and von Mises which are independent of the hydrostatic component of stress. Although these concepts have been found to apply to some geological materials it can not be assumed that they will apply necessarily to pressure-sensitive material such as rocks in which brittle fracture and dilatancy typically occur. Rocks and rock masses often display apparently strain-softening characteristics. The modelling of strain-softening behaviour using plasticity theory presents a number of difficulties. Plasticity is a continuum theory whereas strain-softening in isotropic continuum is impossible theoretically because it intradoses instability. Strain-softening can exist only in a heterogonous material. Heterogeneity in an initially homogeneous material that is deformed uniformly is produced by the localization of shear strain or fracture. Non-normality and non-uniqueness of solution may be associated with such behaviour. It has been found experimentally that an assumption of associated flow overestimates the amount of dilation occurring in yielding rocks (Michelis & Brown 1986). This observation has lead to the development of a number of non-associated flow rules for rocks.

When an associated flow rule applies, the yield criterion and the plastic potential function are the same functions of the stress components. In other words, the flow rule is referred to as associated if the plastic potential and yield surface coincide. As a consequence of this, the plastic strain increment vector must be normal to the yield surface. If the yield surface is represented by a relation between principal stresses, σ_1 and σ_3, then the corresponding components of the strain increment vector are the increments of ε_1^p and ε_3^p. If the flow rule is non-associated, the yield criterion and the plastic potential function are not the same and the normality principles do not apply. There is limited evidence available to suggest that the dilation rate at peak stress in dense brittle rocks or tightly interlocked aggregates can be predicted closely using the associated flow rule. It is not clear, however, that the associated flow rule applies to heavily fractured and poorly interlocked rock masses. Indeed, analyses of data obtained from Brown *et al.*(1983) suggest that, in some such cases, the flow rule will be non-associated. This means that the resulting plastic volume changes will be less than those predicted using an associated flow rule.

According to analyses obtained by an explicit solution undertaken by Wang (1996), it was deduced that calculated results by linear Mohr-Coulomb criterion may overestimate the surface closure in low normal stress, but underestimate the opening closure under high normal stress. For the non-linear case, it was concluded that a non-associated flow rule should be used in general. It is suggested that a nonlinear yield criterion in combination with linear yield potential be used with a non-associated flow rule to achieve an appropriate prediction for the opening surface closure in poor quality rock masses where *GSI < 27*.

More recently, Cundall *et.al* (2004) have already developed a new constitutive model based on new version of Hoek & Brown failure criterion in which the flow rule of plasticity is defined in terms of confining stress level being used. They show that, unlike the past constitutive model, the new flow rule can be express in the case of a variable form, where it is function of confining stress level. For a low confining stress, at which a large rate of volumetric expansion at yield is anticipated, an associated flow rule is applied whereas for high confining stress, at which the material no longer dilates at failure, a constant-volume flow rule (non-associated) is prescribed.

For cases considering the Hoek-Brown material, most of the published analyses take account of a non-associated flow rule with a "constant dilation angle", derived from a "linear" potential. In Hoek-Brown failure criterion, the yield surface is a parabola, and then if the potential is linear, the flow rule will be always non-associated. Note that the different situation as if you have a Mohr-Coulomb (i.e., linear) failure criterion: if the potential is linear and the dilation angle is equal to the friction angle, then both, yield surface and potential are the same, therefore the flow rule is "associated". On the other hand, if the dilation angle is different from the friction angle, then the flow rule will be non-associated.

Depending on the linearity or non-linearity of both the yield function and plastic potential, the following classification given in Table 1-1 can be helpful. As can be seen, there are two natural choices as potential functions for the Hoek-Brown failure criterion:

Table 1-1 Yield and potential functions used in the various tunnel elasto-plastic models

Yield and potential functions	
Linear function	**Non-linear Function**
M-C	**H-B**
F(potential)=F(yield)	**F(potential)=F(yield)**
Linear potential function	Normality and associated flow rule
$\Psi=\Phi$ Associated flow rule	**F(potential)≠F(yield)**
$\psi\neq\Phi$ Non-associated flow rule	Linear potential function
	Non-linear yield function
	Non-associated flow rule
	Constant dilation angle

The first one is to take a potential that has the same form as the yield surface, and this will be the associated flow rule. This case will show the maximum volumetric change possible, also maximum value justifiable in mechanical terms for the plastic state. The second is to take a linear potential with zero dilation angle $Q(\sigma_1,\sigma_3)=0$, and this will be non-associated flow rule. This will show no volumetric change in the plastic state.

In general, the most probable situation will be one between both extreme types of volumetric behaviour in the failure state (associated flow rule and non-dilatant, non-associated).

For poor very weak rock masses (GSI < 27) which is mostly related to the subject of the thesis, Hoek and Brown (1997) suggest taking zero dilation, so, for very weak rock masses, the second alternative defined above is therefore the one to use in this elasto-plastic closed-form solution.

Figure 1-6 shows the linearized plastic potential in the principal stress and plastic strain increment space. As far as a certain stress range is concerned, both the yield surface and the plastic potential may be linearized. For an isotropic material, the principal axes of stress and strain increment coincide, and therefore a plastic strain increment vector AA' ($\dot{\varepsilon}_3,\dot{\varepsilon}_1$) may be plotted. Under plane strain condition, the ratio of plastic strain increment is given by:

Linear plastic potential using Mohr-Coulomb function

$$Q = (\sigma_1 - \sigma_3) - (\sigma_1 + \sigma_3)\sin\phi - 2c\cos\phi = 0 \tag{1-18}$$

or

$$Q = \sigma_1 - \sigma_3 N_\phi + 2c\sqrt{N_\phi} = 0$$

where $N\phi = \dfrac{1+\sin\phi}{1-\sin\phi}$

Using the flow rule (Eq. 1-17), then

$$\varepsilon_1^p = \lambda(1-\sin\phi)$$
$$\varepsilon_3^p = -\lambda(1+\sin\phi) \qquad\qquad (1\text{-}19)$$
$$\frac{\varepsilon_3^p}{\varepsilon_1^p} = -\left(\frac{1+\sin\phi}{1-\sin\phi}\right)$$

In the case of defining the plastic potential, the subscript φ is replaced into ψ to express the role of dilation. The parameter N_ψ controls the inclination of the plastic-strain rate vector represented

$$\frac{d\sigma_1}{d\sigma_3} = -\frac{d\varepsilon_3^p}{d\varepsilon_1^p} = N_\psi \qquad\qquad (1\text{-}20)$$

or

$$d\varepsilon_3{}^p + N_\psi d\varepsilon_1{}^p = 0$$

or in polar coordinate

$$d\varepsilon_r{}^p + N_\psi d\varepsilon_\theta{}^p = 0 \qquad\qquad \mathbf{(1\text{-}21)}$$

where $N_\psi = \dfrac{1+\sin\psi}{1-\sin\psi} = \tan^2(45+\dfrac{\psi}{2})$

Given the plastic part of stress-strain curve of rock (see Figure 1-5) the slope of the plastic part of the axial and lateral strains in plastic region is

$$f = -\frac{d\varepsilon_3^p}{d\varepsilon_1^p}$$

$$(1\text{-}22)$$

Besides, the slope of volumetric strain versus axial strain in the plastic region can be obtained

$$F = f\text{-}1 \qquad\qquad (1\text{-}23)$$

12

Therefore

$$f = 1 + F = N_\psi \tag{1-24}$$

The parameter N_ψ is the dilation coefficient that characterizes the volume change in the plastic zone.   Zero volumetric strain (no volume change) is represented by $N_\psi = 1$ i.e. $\psi = 0$. If $N_\psi = \dfrac{1+\sin\psi}{1-\sin\psi} = \tan^2(45+\dfrac{\psi}{2})$, the associated flow rule is obtained for a Mohr-Coulomb material. For a material with a friction angle of 30°, a value of $N_\psi = 3$ is a upper bound for dilation.

The associated low assumes that the plastic strain increments are normal to the failure envelope (2-D problem) satisfying normality condition, thereby generally overestimates the plastic strains in rock .Therefore, a non-associated flow rule *(1< N_ψ < $\dfrac{1+\sin\psi}{1-\sin\psi}$ m)* is more realistic.

The vector AA' is normal to the plastic potential 'Q' then Q forms an angle $\tan^{-1}N_\psi$ with the ε_3 axis, and satisfies the Equation 1-18.
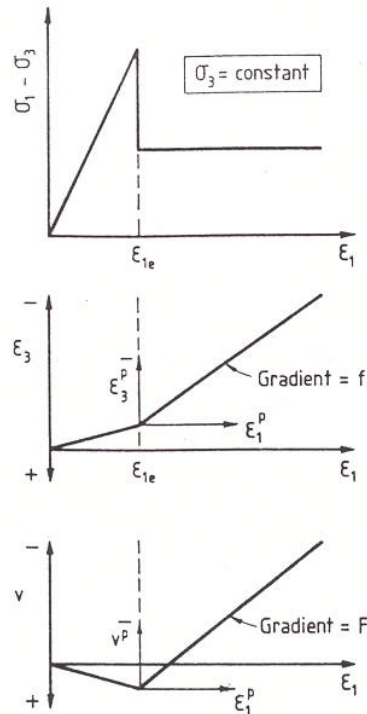
Figure 1-5 Stress-strain regime for a rock obeying elasto-britlle-plastic behaviour
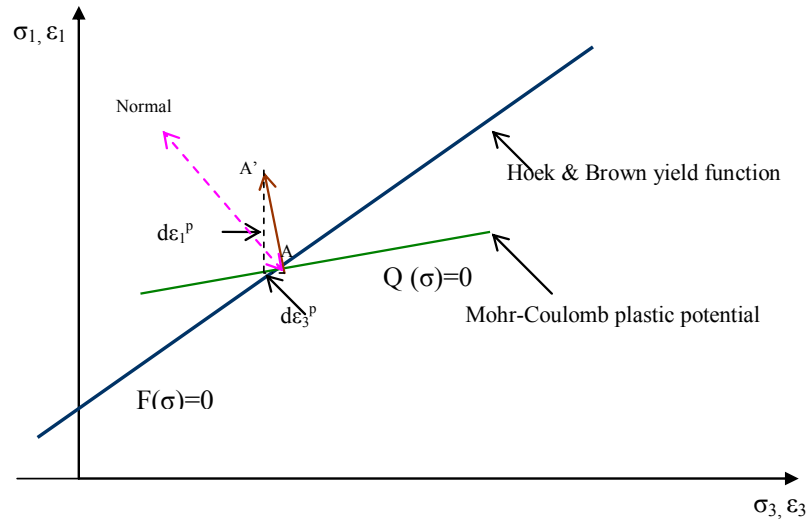
Figure 1-6 Linearized flow rule concept used in this study

1.6   Stress in the plastic zone

The combination of the equilibrium equation and residual failure criterion results in the following ordinary differential equation:

$$\frac{d\sigma_r}{dr} + \frac{\sigma_r - \sigma_\theta}{r} = 0 \tag{1-25}$$

$\tau_{r\theta} = 0$ Axi-symmetrical problem

$$\sigma_\theta = \sigma_r + \sigma_{ci}'\left(m_b' \frac{\sigma_r}{\sigma_{ci}'} + s' \right)^{a'} \tag{1-26}$$

$$\frac{d\sigma_r}{dr} - \frac{\sigma_{ci}'(m_b' \frac{\sigma_r}{\sigma_{ci}'} + s')^{a'}}{r} = 0 \tag{1-27}$$

The shear stress ($\tau_{r\theta}$) at any given radial distance is zero for axisymmetric deformation under plane strain condition. For an unsupported opening where bolt

density parameter ($\beta=0$) and by taking into account the boundary condition at $r=r_i$ $\sigma_r =0$, the solution of non-linear Equation 1-27 is given by:

$$\sigma_r = \frac{\Gamma - s'}{\dfrac{m'_b}{\sigma'_{ci}}} \tag{1-28}$$

$$\Gamma = \left[s'^{1-a'} - m'_b (a'-1)\ln\left(\frac{r}{r_i}\right)\right]^{\frac{1}{1-a'}} \tag{1-29}$$

In literature some analytical solutions, mostly based on the convergence-confinement method, used the internal pressure (P_i) as the effect of the fictitious support pressure that imposes of the tunnel boundary. In such a case, in order to draw the ground characteristic curve the support pressure must decrease gradually as the convergence increases. For this case, the solution of non-linear Equation 1-27 is obtained by taking into consideration the boundary condition at $r=r_i$, $\sigma_r =P_i$:

$$\sigma_r = \frac{\dfrac{\Omega}{\sigma'_{ci}} - s'}{\dfrac{m'_b}{\sigma'_{ci}}} \tag{1-30}$$

$$\Omega = \left[(m'_b P_i + \sigma'_{ci} s')^{1-a'} - m'_b (a'-1)\sigma'^{1-a'}_{ci} \ln\left(\frac{r}{r_i}\right)\right]^{\frac{1}{1-a'}} \tag{1-31}$$

1.7 Stress in the outer elastic zone

In the elastic zone, the stress distributions are given by classical Lame's solution as follows:

$$\sigma_\theta = P_o + (P_o - \sigma_{re})\left(\frac{r_e}{r}\right)^2 \text{ or } \sigma_\theta = P_o\left[1+\left(\frac{r_e}{r}\right)^2\right] - \sigma_{re}\left(\frac{r_e}{r}\right)^2 \tag{1-32}$$

$$\sigma_r = P_o - (P_o - \sigma_{re})\left(\frac{r_e}{r}\right)^2 \text{ or } \sigma_r = P_o\left[1-\left(\frac{r_e}{r}\right)^2\right] + \sigma_{re}\left(\frac{r_e}{r}\right)^2 \tag{1-33}$$

where σ_{re} is the radial stress at the elastic-plastic interface.

15

The stress distribution in the elastic zone is equivalent to that of a larger opening of radius r_e, supported by a uniform internal stress σ_{re} under the same external field stress. r_e is the radial distance to the outer limit of the yielding zone surrounding the opening.

At the elastic-plastic boundary ($r=r_e$), the internal stresses are given by from plastic part:

$$\sigma_{re} = \frac{\Delta - s'}{\dfrac{m_b'}{\sigma_{ci}'}} \tag{1-34}$$

$$\Delta = \left[s'^{1-a'} - m_b'(a'-1)\ln\left(\frac{r_e}{r_i}\right) \right]^{\frac{1}{1-a'}} \tag{1-35}$$

From elastic part at $r=r_e$ the Equations 1-32 and 1-33 can be arranged as:

$$\sigma_{\theta e} - \sigma_{re} = 2(P_o - \sigma_{re}) \tag{1-36}$$

$$\sigma_{\theta e} + \sigma_{re} = 2P_o \tag{1-37}$$

Using the peak strength criteria for elastic-plastic boundary:

$$\sigma_{\theta e} - \sigma_{re} = \sigma_{ci}\left(m_b \frac{\sigma_{re}}{\sigma_{ci}} + s \right)^a \tag{1-38}$$

Equating 1-36 and 1-38 yields the following non-homogeneous equation:

$$2(P_o - \sigma_{re}) = \sigma_{ci}\left(m_b \frac{\sigma_{re}}{\sigma_{ci}} + s \right)^a \tag{1-39}$$

A closed-form (exact) solution is only possible when $a = 0.5$. However, numerical methods (approximate solution), like the Newton-Raphson method, can be applied to approximate the exact solution to Equation 1-39 (Press, Flannery, Teukolsky, & Vetterling, 1994). Subsequently, the Equation 1-39 is independently solved when $a = 0.5$

$$\sigma_{re} = P_o + \frac{m_b \sigma_{ci}}{8} \pm \frac{1}{8}\sqrt{16 P_o m_b \sigma_{ci} + m_b{}^2 \sigma_{ci}{}^2 + 16 \sigma_{ci}{}^2 s} \qquad (1\text{-}40)$$

Negative subtraction of above equation is acceptable and after abbreviating

$$\sigma_{re} = P_o - M \sigma_{ci} \qquad (1\text{-}41)$$

$$M = \frac{1}{2}\left[\left(\frac{m_b}{4}\right)^2 + m_b \frac{P_o}{\sigma_{ci}} + s\right]^{\frac{1}{2}} - \frac{m_b}{8} \qquad (1\text{-}42)$$

1.8   Radius of the plastic zone

The plastic zone radius r_e can be determined by assuming continuity of radial stress at the elastic-plastic boundary. It is also assumed that the field boundaries are far enough from the opening, such that their influence on the solution on the solution for r_e is negligible.

Equating the expressions 1-34 and 1-40 (for σ_{re} at $r = r_e$), the normalized plastic zone radius (r_e/r_i) can be derived as follows:

$$\frac{r_e}{r_i} = e^X \qquad (1\text{-}43)$$

$$X = \frac{s'^{1-a'} - \left\{s' + \frac{P_o m_b'}{\sigma_{ci}'} + \frac{m_b m_b' \sigma_{ci}}{8 \sigma_{ci}'} - \frac{m_b'}{8 \sigma_{ci}'}\left(16 P_o m_b \sigma_{ci} + m_b{}^2 \sigma_{ci}{}^2 + 16 \sigma_{ci}{}^2 s\right)^{\frac{1}{2}}\right\}^{1-a'}}{m_b'(a'-1)}$$

1.9   Strains and displacement analysis

1.9.1   Strains in elastic zone

Hook's laws can be applied to determine the radial and tangential strains in the elastic region surrounding the plastic zone (Timoshenko & Goodier, 1970):

17

$$\varepsilon_r = \frac{1-\nu^2}{E}\left[\sigma_r - \left(\frac{\nu}{1-\nu}\right)\sigma_\theta\right] \tag{1-44}$$

$$\varepsilon_\theta = \frac{1-\nu^2}{E}\left[\sigma_\theta - \left(\frac{\nu}{1-\nu}\right)\sigma_r\right] \tag{1-45}$$

$$\gamma_{r\theta} = \frac{1}{G}\tau_{r\theta} \tag{1-46}$$

Under axi-symmetrical condition

$$\varepsilon_z = 0, \gamma_{zx} = \gamma_{zy} = 0, \gamma_{r\theta} = 0 \, and \, \tau_{r\theta} = 0$$

$$\tau_{zx} = \tau_{zy} = 0$$

Recalling stresses in elastic zone (Equations 1-32 and 1-33) and substituting into Equations 1-44 and 1-45 provide the strain field for under plane strain condition

$$\varepsilon_r = \frac{(1-2\nu)}{2G}P_o + \frac{(\sigma_{re} - P_o)}{2G}\left(\frac{r_e}{r}\right)^2 = \frac{(1-2\nu)}{2G}P_o - \frac{M\sigma_{ci}}{2G}\left(\frac{r_e}{r}\right)^2 \tag{1-47}$$

$$\varepsilon_\theta = \underbrace{\frac{(1-2\nu)}{2G}P_o}_{\substack{\text{Elastic} \\ \text{deformation}}} \underbrace{- \frac{(\sigma_{re} - P_o)}{2G}\left(\frac{r_e}{r}\right)^2}_{\substack{\text{Deformation due to} \\ \text{excavation}}} = \frac{(1-2\nu)}{2G}P_o + \frac{M\sigma_{ci}}{2G}\left(\frac{r_e}{r}\right)^2 \tag{1-48}$$

1.9.2 Strains in plastic zone

The total strains in the plastic zone are made up of both elastic and plastic strains as given by the Equation 1-4. Hook's law and flue rule have been applied to calculate the elastic and plastic strains, respectively. Expanding the Equation 1-4 under plane strain condition yields

$$\varepsilon_\theta^t = \varepsilon_\theta^e + \varepsilon_\theta^p$$
$$\varepsilon_r^t = \varepsilon_r^e + \varepsilon_r^p \tag{1-49}$$

18

It should be, at this point, noted that the elastic strains are very small compared to the plastic strains.

1.9.2.1 Determination of the elastic strains in the plastic zone

Using generalized Hook's law (Equations 1-44 and 1-45) and substituting stresses in the plastic zone (Equations 1-26 and 1-28):

$$\varepsilon_r^e = \frac{1}{2G}\left[(1-2v)(\frac{\Gamma - s'}{\dfrac{m_b}{\sigma_{ci}'}}) - v\sigma_{ci}'\Gamma^{a'}\right] \tag{1-50}$$

$$\varepsilon_\theta^e = \frac{1}{2G}\left[(1-2v)(\frac{\Gamma - s'}{\dfrac{m_b}{\sigma_{ci}'}}) + (1-v)\sigma_{ci}'\Gamma^{a'}\right] \tag{1-51}$$

Then

$$\varepsilon_\theta^e - \varepsilon_r^e = \frac{1}{2G}\sigma_{ci}'\Gamma^{a'} \tag{1-52}$$

1.9.2.2 Determination of the plastic strains in the plastic zone

Substituting the Equations 1-50 and 1-51 in the strain compatibility (Equation 1-3) and taking account of the flow rule (Equation 1-17) provide the following non-linear differential equation:

$$\frac{d\varepsilon_\theta^p}{dr} + \frac{\sigma_{ci}'}{2Gr}\left[s'^{1-a'} - m_b'(a'-1)\ln\left(\frac{r}{r_i}\right)\right]^{\frac{a'}{1-a'}}\left[(1-2v)+a'm_b'(1-v)\right] +$$
$$\frac{1}{r}\left[\varepsilon_\theta^p(1+N_\psi)+\frac{\sigma_{ci}'}{2G}\left[s'^{1-a'}-m_b'(a'-1)\ln(\frac{r}{r_i})\right]^{\frac{a'}{1-a'}}\right]=0 \tag{1-53}$$

The boundary condition used in solving Equation 1-53 can be written as:

$$\varepsilon_\theta^p = \frac{M\sigma_{ci}}{2G} \text{ at } r = r_e$$

Even though it is first order, the non-liner Equation 1-53 can be solely solved by the numerical methods provided by some packages such as MATEMATICA or MAPLE. The solution of the Equation 1-53, considering the prescribed boundary condition, will be as below:

$$\varepsilon_\theta^p = \frac{1}{r^{1+N_\psi}} \left[\begin{array}{l} \dfrac{M\sigma_{ci}}{2G} r_e^{1+N_\psi} + \\[2mm] \left(\dfrac{\sigma_{ci}'}{2G}(1-\nu)(2+a'm_b') \right) \displaystyle\int_r^{r_e} r^{N_\psi-1} \left[s'^{1-a'} + m_b'(1-a')\ln\left(\dfrac{r}{r_i}\right) \right]^{\frac{a'}{1-a'}} dr \end{array} \right] \quad (1\text{-}54)$$

As can be seen from Equation 1-54, an integral function has been introduced in the result of the differential equation. The complete solution can be obtained provided that the integral on the right side of the Equation 1-54 is evaluated numerically as represented in the Appendix A.

1.9.2.3 Radial displacement field

The displacement field can be obtained directly by the following strain-displacement relationships which satisfy the compatibility conditions:

$$\varepsilon_\theta = \frac{u_r}{r} + \frac{1}{r} \cdot \frac{\partial u_\theta}{\partial \theta}$$

$$\varepsilon_r = \frac{\partial u_r}{\partial r} \quad (1\text{-}2)$$

The conditions of plane strain under axi-symmetric deformation ($\gamma_{r\theta}$) imply that the total strains are independent of the tangential strain components. Therefore, the radial displacement field can be readily evaluated from any of the following expressions:

$$\frac{u_r}{r} = \varepsilon_\theta^t \quad \text{or} \quad u_r = \int \varepsilon_r^t dr \quad (1\text{-}55)$$

The displacement field is then given by:

$$\frac{u_r}{r} = \frac{1}{2G}\left[\begin{array}{l}(1-2\nu)(\dfrac{\Gamma - s'}{\dfrac{m'_b}{\sigma'_{ci}}}) + (1-\nu)\sigma'_{ci}\Gamma^{a'} + \dfrac{M\sigma_{ci}}{r^{1+N\psi}}r_e^{(1+N\psi)} + \\[20pt] \dfrac{1}{r^{(1+N\psi)}}\sigma'_{ci}(1-\nu)(2+a'm'_b)\displaystyle\int_r^{r_e} r^{N_\psi - 1}\Gamma^{a'}dr \end{array}\right] \qquad (1\text{-}56)$$

where Γ can be obtained from Equation 1-29 as below

$$\Gamma = \left[s'^{1-a'} - m'_b(a'-1)\ln\left(\frac{r}{r_i}\right)\right]^{\frac{1}{1-a'}} \qquad (1\text{-}29)$$

Subsequently, elasto-plastic tunnel surface convergence can be subsequently determined by substituting $r=r_i$ in the above expressions.

$$\frac{u_r}{r_i} = \frac{1}{2G}\left[\begin{array}{l}(1-\nu)\sigma'_{ci}s'^{a'} + \dfrac{M\sigma_{ci}}{r_i^{1+N\psi}}r_e^{(1+N\psi)} + \\[20pt] \dfrac{1}{r_i^{(1+N\psi)}}\sigma'_{ci}(1-\nu)(2+a'm'_b)\displaystyle\int_{r_i}^{r_e} r^{N_\psi - 1}\Gamma^{a'}dr \end{array}\right] \qquad (1\text{-}57)$$

Neglecting elastic strain due to its very small magnitude in comparison with plastic strain, the above equation will be simplified as:

$$\frac{u_r}{r_i} = \frac{1}{2G}\left[\begin{array}{l}\dfrac{M\sigma_{ci}}{r_i^{1+N\psi}}r_e^{(1+N\psi)} + \\[20pt] \dfrac{1}{r_i^{(1+N\psi)}}\sigma'_{ci}(1-\nu)(2+a'm'_b)\displaystyle\int_{r_i}^{r_e} r^{N_\psi - 1}\Gamma^{a'}dr \end{array}\right] \qquad (1\text{-}58)$$

Appendix B presents the spreadsheet form of a practical example to be solved by the proposed elasto-plastic solution.

1.10 Convergence- confinement method

The principles of the method can be outlined briefly here. Initially the ground is assumed to be naturally stressed at a hydrostatic P_o pressure and a tunnel of radius r_i is excavated. Assuming a point in the periphery of the opening as a reference point, some inward displacement (towards the tunnel axis) will be recorded as the tunnel face progresses towards the point of reference. This deformation can be simulated by the action of equivalent pressure acting internally in the opening which can be expressed as a fraction of the initial in situ P_o stress. This is called the "equivalent support pressure" since it gives the same radial deformation or otherwise known as "pre-convergence". From the initial pressure P_o the ground is gradually unloaded (relaxed) and for some time it behaves elastically. If the ground reaches its strength, further unloading causes the mass to deform plastically and a failure zone is formed around the opening. If at a certain distance d from the face of the tunnel support is installed, then the support pressure versus support deformation plot can be plotted on the same coordinate system as the characteristic curve. The intersection of the two curves is presumably the point of equilibrium for the ground and support assuming that no secondary effects such as creep or long term strength loss occur in the ground. More recently, the convergence-confinement method has been critically reviewed and well-assessed in connection with various support and reinforcement systems by Carranza-Torres and Fairhust (2000), Oreste and Peilla (1996), Oreste (2002, 2003), Peila and Oreste(1995), Peila *et al.* (1997).

Perhaps the most critical points in the above method are estimating how much deformation (or relaxation) has occurred in the rock mass prior to the installation of the support. The knowledge of this pre-deformation would allow positioning the support curve at the right origin on the horizontal axis. Panet & Guenot (1982) reviewed the problem of the radial deformations along the length of a tunnel by using measured data and at the same time by conducting parametric analysis using simple axi-symmetric formulations. In the following parts we will see that the final displacement obtained from the proposed analytical model could be referred as the deformation prior to the installation of the support.

According to Panet & Guenot (1982), convergence of the tunnel can be expressed as a function of several parameters including the distance of the assumed point from the tunnel face, the unsupported distance behind the face and the stiffness of the support system. The convergence – confinement method attempts to associate the convergence of the tunnel with the distance from the tunnel since if such a relation is known then any pre-convergence that has occurred before the support is installed and becomes effective, can be estimated. This is the mechanism exploited by the NATM philosophy and the fact that can lead to economic designs since timing of installation will determine the amount of picked up loads carried by the structural components of the support. The equivalent pressure pi is expressed as a function of the in-situ pressure by the use of the confinement loss factor λ:

$$P_i = (1-\lambda)P_o \qquad\qquad\qquad\qquad (1\text{-}59)$$

The parameter λ varies from 0 for initial conditions, to 1 for a full excavated tunnel and equilibrium conditions. To the present various authors have suggested the use of some approximation for the estimation of the convergence ratio: $C(x) / C(\infty)$, where $C(x)$ is the convergence at a distance x from the face and $C(\infty)$ is the final far away from the tunnel face. For unsupported tunnels in elastic ground this ratio is function of the tunnel radius and for yielding ground this is a function of the plastic parameters of the ground which affect the plastic radius developed around the tunnel.
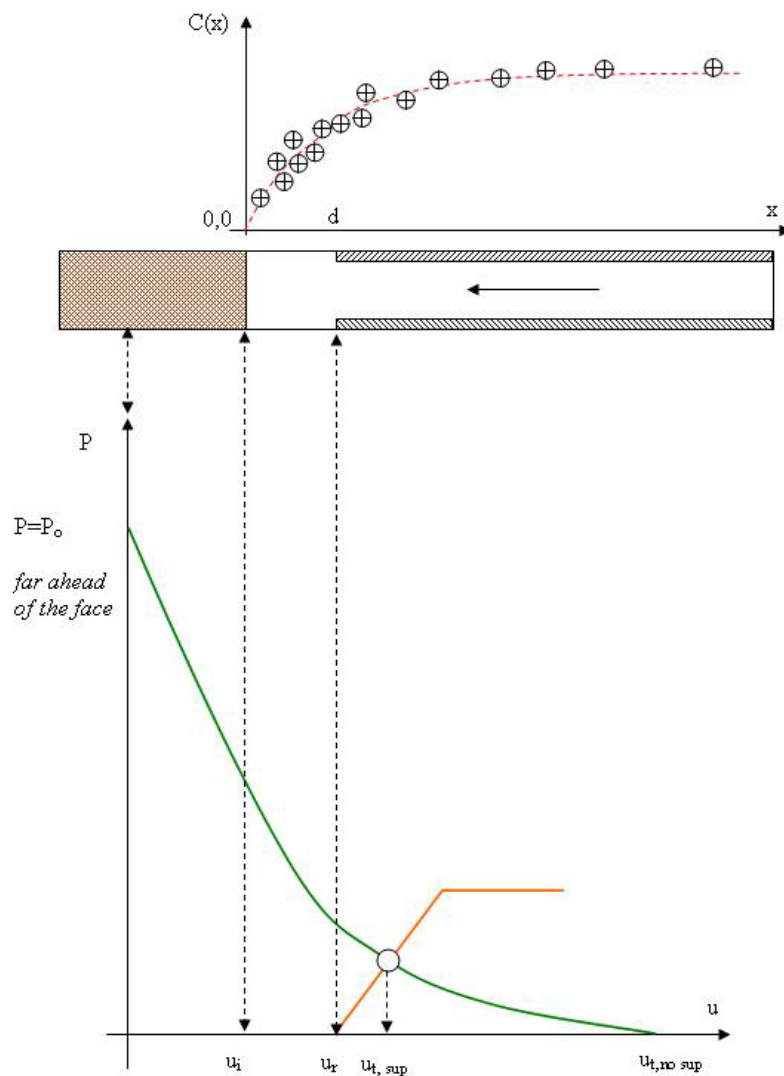
Figure 1-7 Schematic representation of the Convergence-Confinement concept along with longitudinal convergence profiles.

1.11 Validation of the proposed elasto-plastic model by numerical modelling

There is often advantage in being able to validate the results of analytical solution with those of numerical modelling. In this chapter, as a check on the analytical results and in order to ensure the feasibility of the proposed analytical elasto-plastic model, a numerical analysis is carried out using the Finite Difference Code (Fast Lagrangian of Continua "FLAC") and both results will be compared.

A quarter symmetry and axi-symmetrical models are to be carried out in this part. The adopted geomechanical parameters used here is represented in Table 1-2.

Table 1-2 Input parameters used in numerical modelling

Rock mass properties used in numerical modelling	
r_i(m)	2
Po (MPa)	15
E(Gpa)	5.7
ν	0.3
σci	30
ψ	0
mb	1.7
s	3.90E-03
mb'	0.85
s'	1.90E-03
a	0.5
S	1
σci'	27
r(m)	2
a'	0.5
Nψ	1.0

1.11.1 Numerical modelling of a unsupported tunnel (Quarter symmetry model)

A two-dimensional plane-strain FLAC model with the plane of analysis oriented normal to the axis of the hole is created for this problem. For this model, only a quarter of the problem needs to be analyzed because of the symmetry of the problem (quarter-symmetry). The model and boundary conditions are shown in Figure 1-8. In FLAC analysis the area representing the problem is divided into finite-difference zones, as shown in Figure 1-8. A total of 14400 zones (120 * 120) are used in this grid. The location of the boundary was varied to evaluate its effect on solution accuracy. The boundary is at 30 m (i.e., 15 times the tunnel radius width and height) from the tunnel axis.

The validity proposed elasto-plastic model of circular tunnel satisfying the latest version of Hoek & Brown failure criterion must be tested by numerical

approach (FLAC codes). Therefore, it is appropriate that the stresses and displacements be determined for the case of a cylindrical tunnel in an infinite Hoek-Brown medium subjected to an in-situ stress field.

The problem is based on the data used in Table 1-2.The strength is assumed to reduce after failure initiates; this is simulated by assigning a different set of Hoek-Brown properties for material that has failed (broken material) versus material that has not failed (intact material).
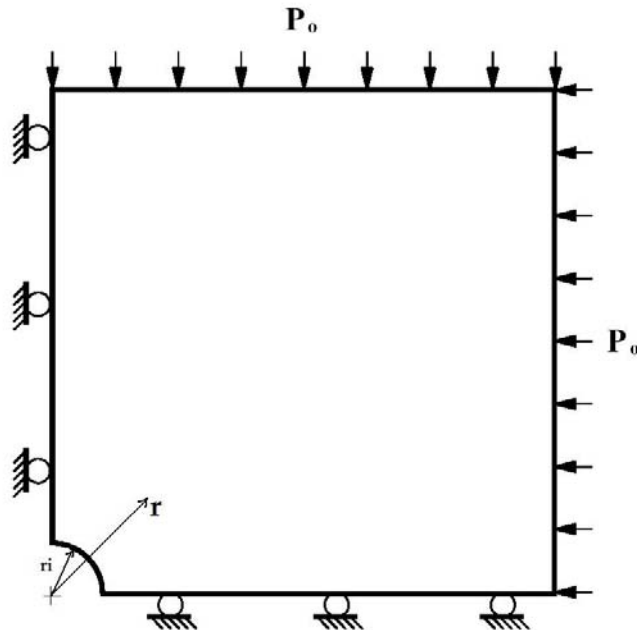
Figure 1-8 Model for FLAC analysis of a circular tunnel in an infinite Hoek &Brown medium- quarter symmetry model

This problem demonstrates the implementation of a *FLAC* constitutive model that has been modified with *FISH*. The Mohr-Coulomb failure surface is adjusted to approximate the Hoek-Brown failure surface. Figure 1-9 to Figure 1-12 are the plots of FLAC output for the geomechanical parameters summarized in Table 1-2. Plots of the stress imposed on roof or tunnel, of the displacement, of the plastic zone extension, and of the displacement trajectory have validated the numerical modelling in quarter symmetry model.

Figure 1-13 shows the radial and tangential stresses calculated by *FLAC*, compared to the analytical solution for σ_r, and σ_θ for the quarter-symmetry model and the *FLAC* results are essentially identical for the quarter-symmetry model. The displacement field near the tunnel for both analytical and numerical methods is displayed in Figure 1-14. It can be observed that there is a good agreement between the proposed model and the *FLAC* results.

A significant result to be noted is that the displacement of proposed analytical solution varies considerably with the variation of the constant a of Hoek

& Brown failure criterion with the quality of rock mass. Unlike most of the existing elasto-plastic solutions for tunnel problems in Hoek-Brown media that consider an intact rock (i.e., a = 0.5),the proposed elasto-plastic solution for the axi-symmetrical problem of excavating a circular tunnel in generalized Hoek-Brown material adopts the value of (a) in accordance with rock mass quality (i.e., $a \geq 0.5$). The differences between the displacements filed near the tunnel are presented in the Figure 1-15. As the magnitude of "a" increases proportionally with decreasing rock mass quality, a drastic increases in tunnel wall displacement is evident. The ground reaction curve (GRC) of the unsupported tunnel built based on proposed elasto-plastic model is represented in Figure 1-16.
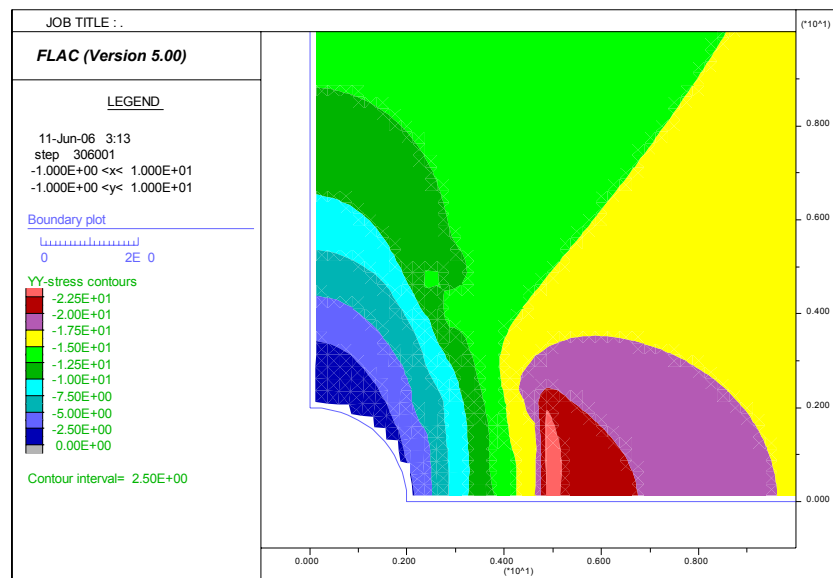
Figure 1-9 Stress in Y-direction indicating the support pressure at the roof of tunnel in quarter symmetry model

1.11.2 Axi-symmetrical elasto-plastic model for unsupported circular tunnel

The aim of this analysis is to monitor the displacement (convergence) near the face of an advancing tunnel using FLAC code. A circular tunnel is sequentially excavated in rock mass with geomechanical properties presented in Table 1-2. The aim of this exercise is to determine the displacements that take place before the lining is installed. Further, the ultimate displacement behind the face is obtained regardless of the 3-D face effect. This type of information can then be used to enable a two-dimensional plane-strain analysis to include the effect of tunnel advancement on relaxation of tunnel loads. Also the longitudinal displacement profile can be resulted from this analysis. Since the displacement at the time of support installation is around 30 % of total displacement, using the ground reaction curve the required support pressure can be acquired, which is a significant parameter in convergence-confinement method.
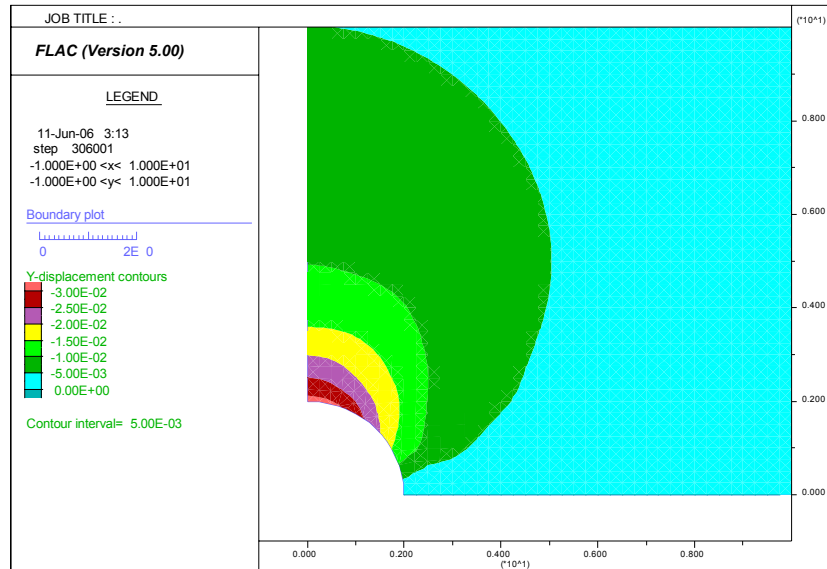
Figure 1-10 Displacement in Y-direction in quarter symmetry model
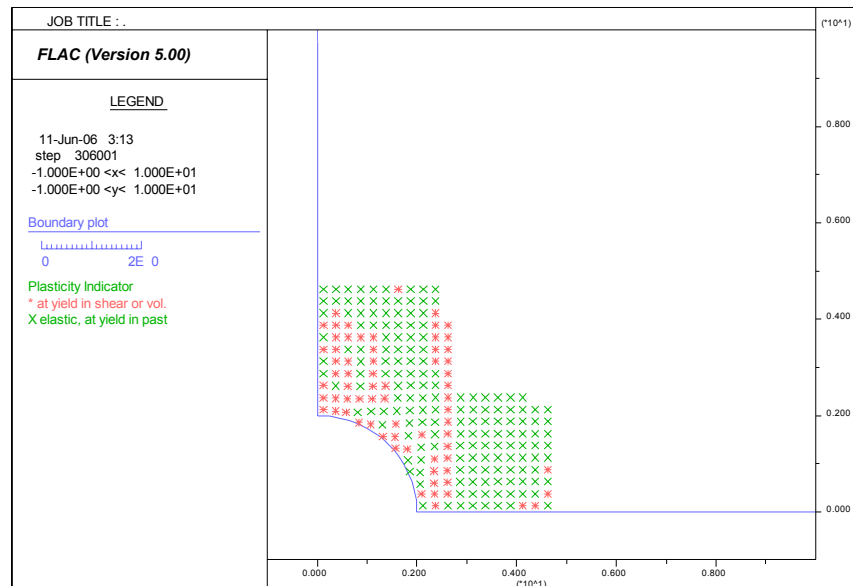
Figure 1-11 Plastic zone extension around the tunnel in quarter symmetry model
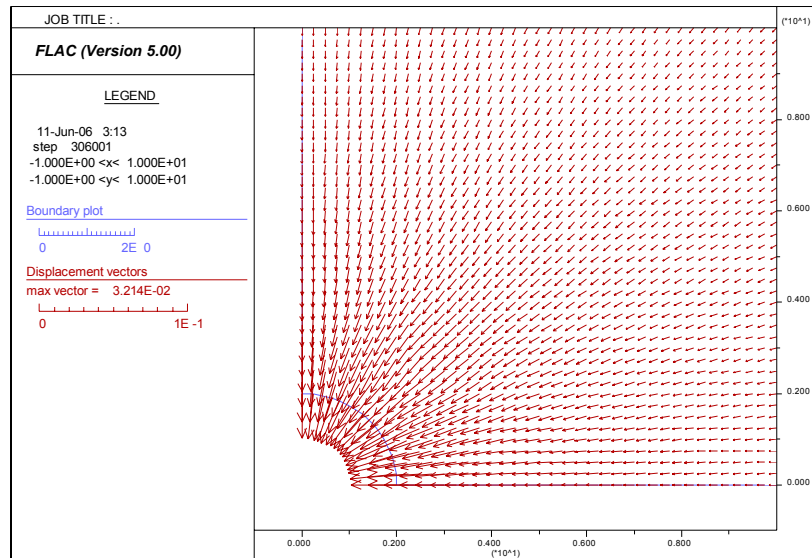
Figure 1-12 Displacements trajectories in quarter symmetry model
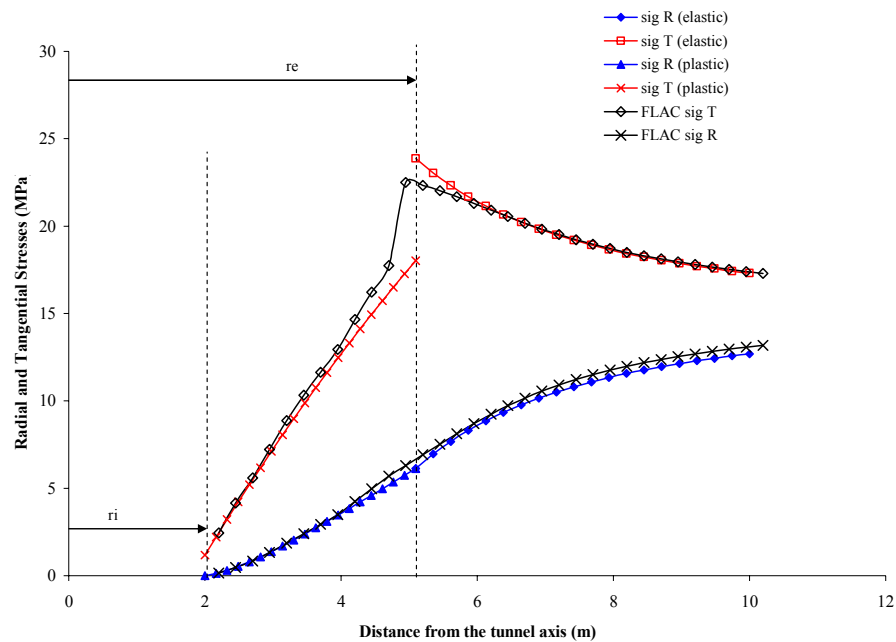
Figure 1-13 Tangential and radial stress filed result from the analytical and numerical methods
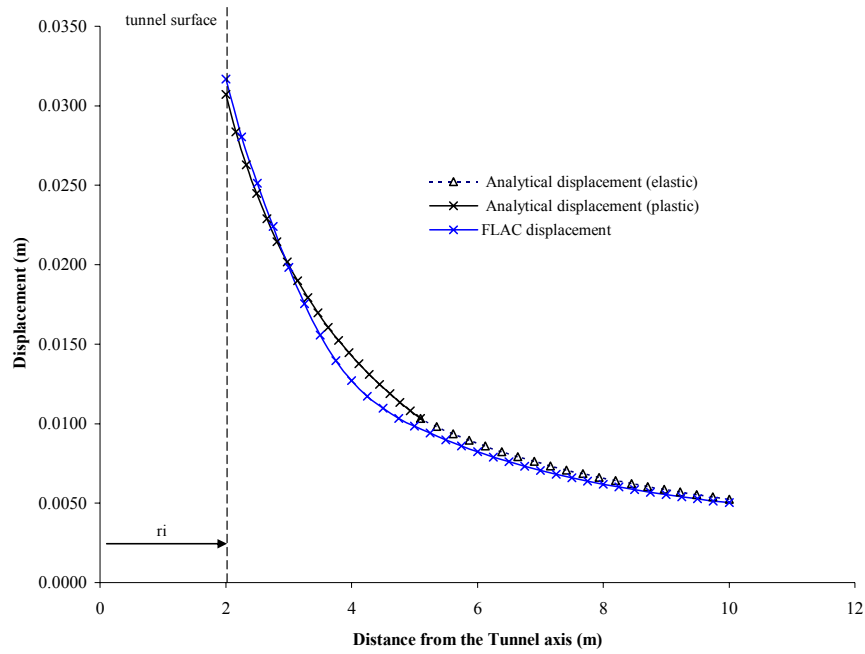
Figure 1-14 Displacement filed stems from the analytical and numerical methods
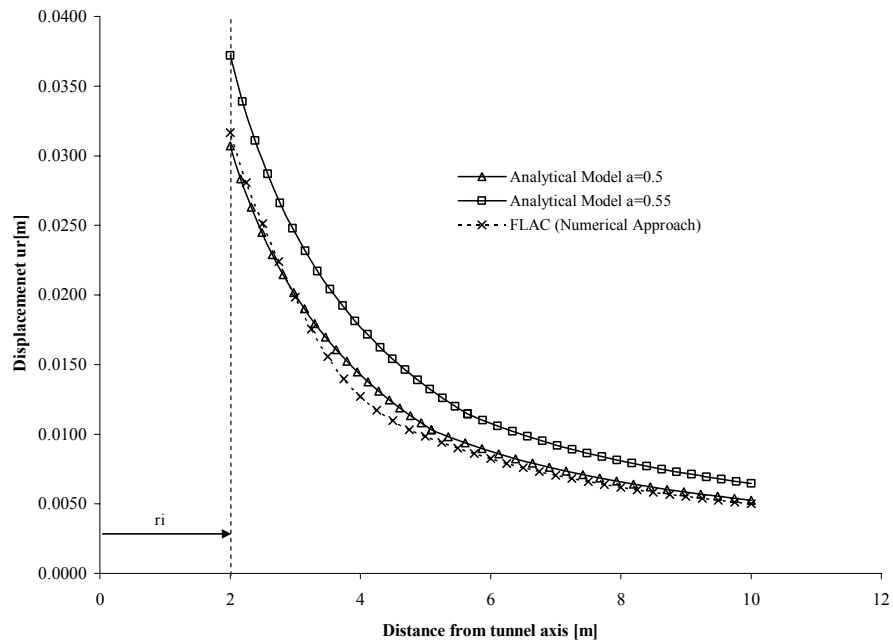
Figure 1-15 Variation of the displacements with different value of Hoek & Brown constant (*a*).
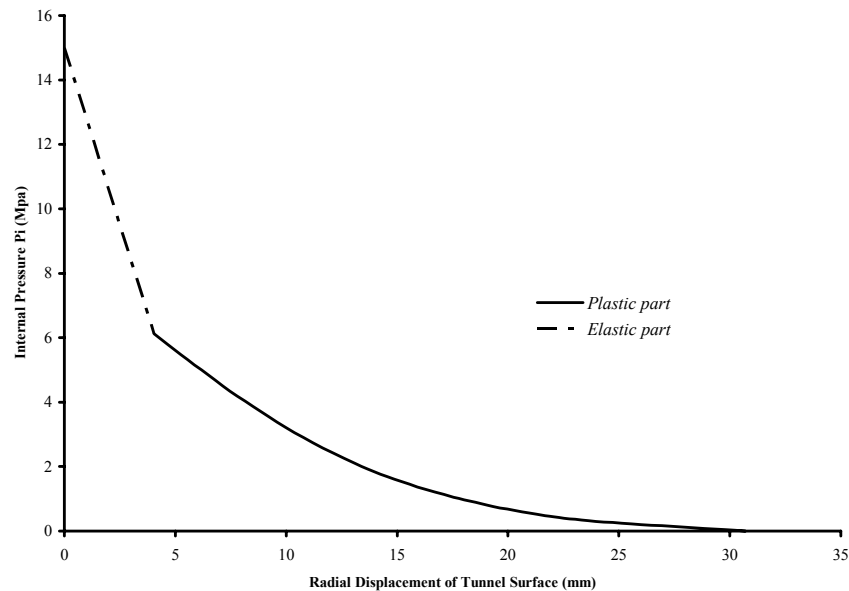
Figure 1-16 Ground Reaction Curve (GRC) of tunnel example based on elasto-plastic model

For this example, the tunnel's diameter is 4 m. The excavation increments are 1 m long. Figure 1-17 shows a cross section view of the sequential excavation.

Because the axis of the tunnel is an axis of radial symmetry, an axisymmetric model is used in this example. The *FLAC* model has dimensions 72 m by 80 m (grid 87 *160) and contains 13920 zones. Six times of tunnel diameter behind and ahead of the face are modelled so as to be able to depict the longitudinal displacement profile. The displacement at the face is recorded at i=5 j=81 for each step of excavation. A total of 52 steps are carried out. Figure 1-18 shows the zone geometry at the end of the run.

Panet & Guenot (1982) have presented numerical analyses of the advancing face effect (k=1) for circular tunnels driven through elasto-plastic material. In their solutions, the prediction of the convergence profile behind the face requires a preliminary assessment of the ultimate time-independent closure and the final extent of the plastic zone. Alternatively, several in-situ convergence measurements behind the face may be utilized for the purpose of semi-empirical solution. However, the ultimate convergence and the corresponding plastic zone radius for both unsupported and reinforced openings can be determined by the analytical solution proposed in this thesis. Consequently, the 3-D convergence response near the tunnel face may be extrapolated from the ultimate time-independent behaviour.

The proposed elasto-plastic solution predicts the ultimate convergence (more than two tunnel diameter behind the face). 3-D effects close to the face have been neglected. In reality, the observed convergence (u_r) is affected by the face

effects, and is generally less than the predicted total convergence (u_t) by the amount of displacement (u_i) which occurs ahead of the face or prior to initial measurement. The ultimate displacements behind tunnel face are obtained to be 27.9 mm and 25.2 mm by analytical and numerical methods, respectively. The displacement (convergence) at face is about 30 % of the total displacement as shown in Figure 1-19. Some important plots of FLAC analysis indicating displacement trajectories, displacement counters, and plastic zone extension are outlined in Figure 1-20 to Figure 1-22.
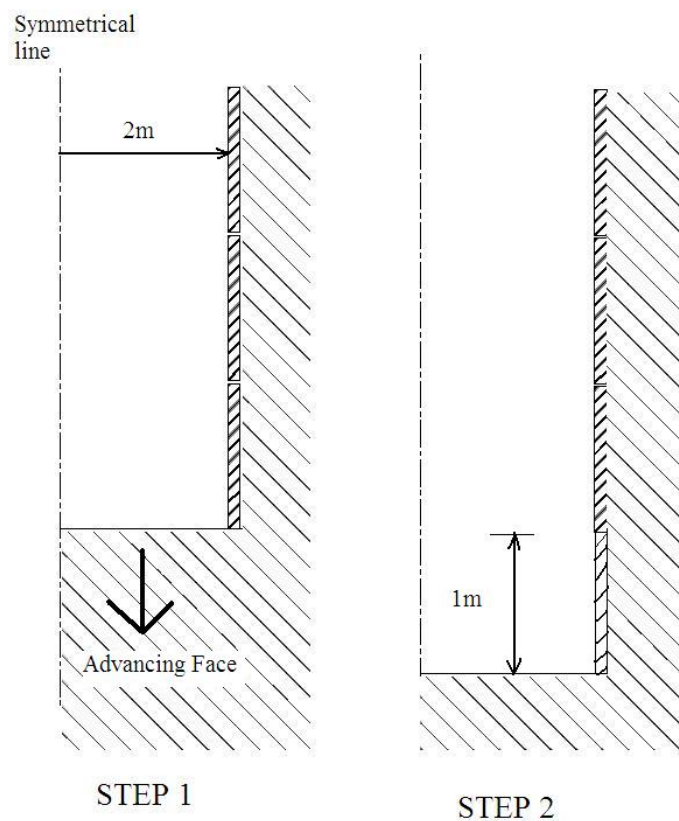
Figure 1-17 Problem geometry and excavation steps
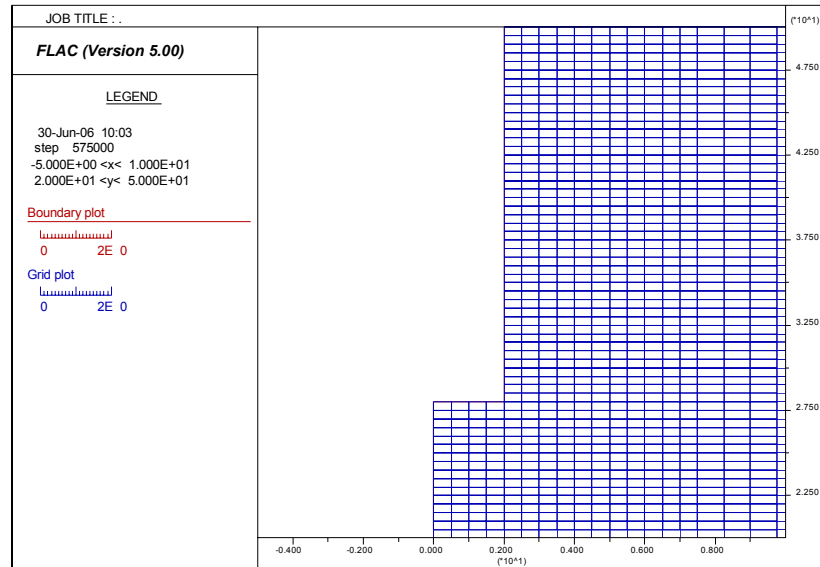
Figure 1-18 Zone geometry (detail) of the axi-symmetrical model
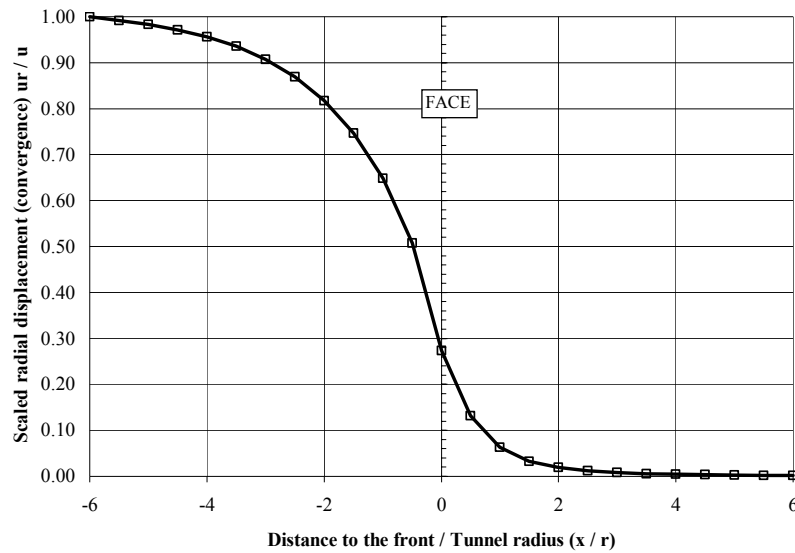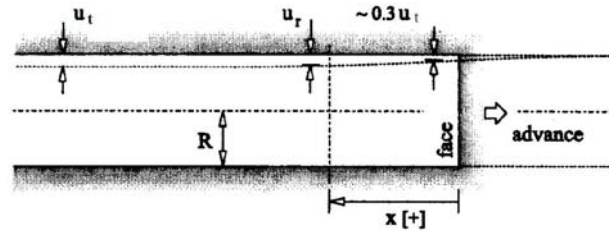
Figure 1-19 Profile of radial displacements u_r for an unsupported tunnel in the vicinity of the tunnel face
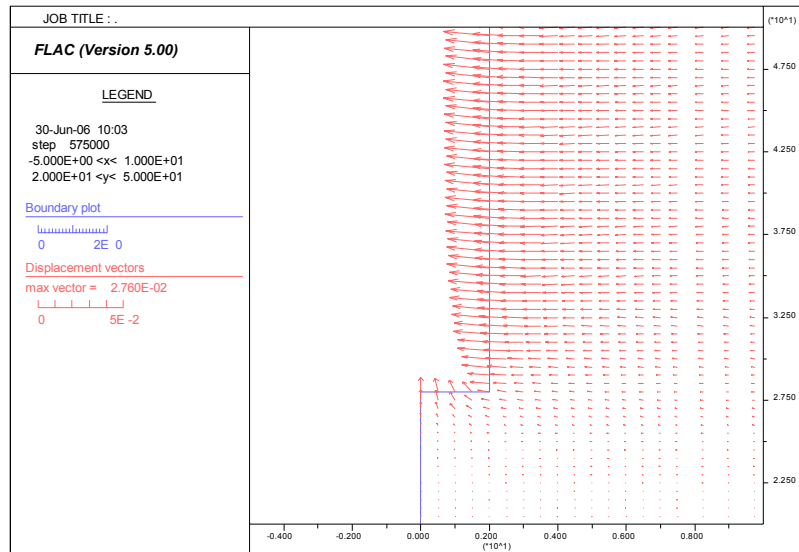
Figure 1-20 Displacement trajectories at the face (intrusion) and at the wall (convergence) in axi-symmetrical model of tunnel
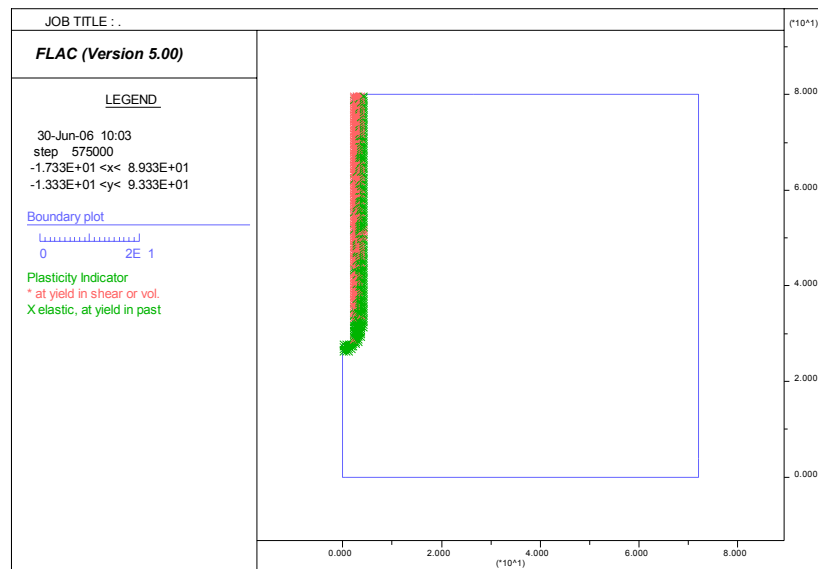
Figure 1-21 Symmetrical plastic zone around the axi-symmetrical tunnel model
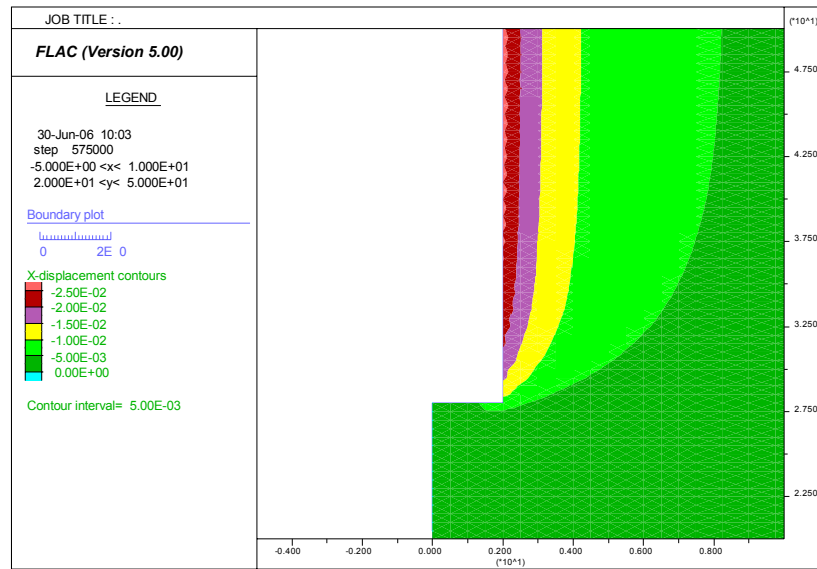
Figure 1-22 Displacement in x-direction. The final displacement behind the tunnel face can be observed.

CHAPTER 2

2 ELASTO-PLASTIC SOLUTION FOR TUNNEL REINFORCEMENT DESIGN

2.1 Introduction

In Chapter 1, the axi-symmetrical analytical elasto-plastic formulations in the case of unsupported tunnel which is being excavated in natural rock mass have been introduced. In this chapter, the same problem will be investigated when the tunnel is reinforced by radial passive grouted rock bolts. The equivalent strength material approach is taken into account in such a way that the strength parameters of rock mass are uniformly improved as the result of the bolting effect. Finally, the Ground Reaction Curve (GRC) of reinforced tunnel, main component of convergence-confinement method, is readily built.

2.2 Stress distribution along fully grouted bolts

The shear stress distribution (τ_z) along a grouted bolt can be represented by (Xueyi, 1983):

$$-dQ_z = \pi d \tau_z dz \tag{2-1}$$

$$\tau_z = -\frac{1}{\pi d} \cdot \frac{dQ_z}{dz} = -\frac{r_b}{2} \cdot \frac{d\sigma_z}{d_z} \tag{2-2}$$

where bolt diameter $d=2 \times$ *bolt radius (r_b)*, Q_z is the axial load distribution and σ_z is the axial stress distribution along the bolt.

The shear stress is related to the first derivative of the axial stress; hence, a zero value of τ_z defined as the neutral point must exist where the axial stress attains a maximum. A model for stress distribution associated with grouted bolts has been proposed initially by Freeman (1978) based on field measurements from the Kielder experimental opening, and later by Xueyi (1983), also based on field observations. This model, illustrated diagrammatically in Figure 2-1, clearly demonstrates the occurrence of the neutral point at the location of the maximum

axial stress. It further exhibits points of inflection on the axial stress distribution associated with the maximum and minimum of the shear stress distribution, where:
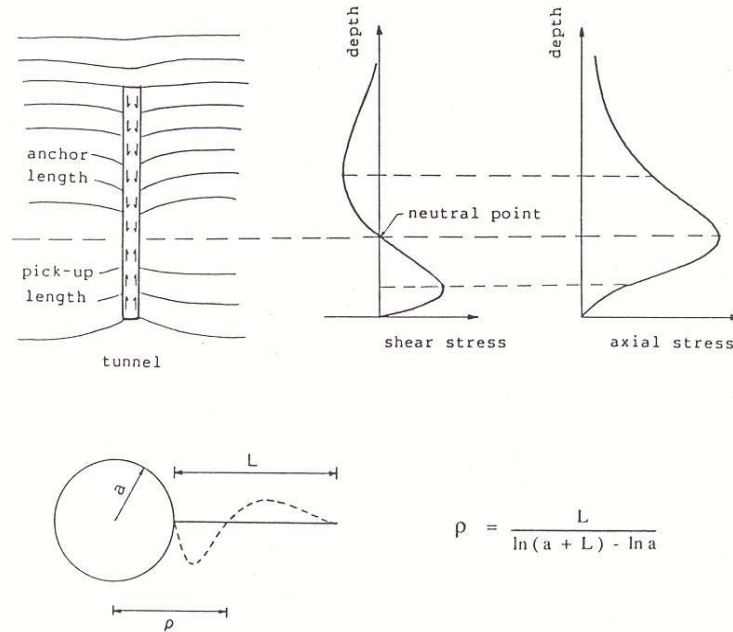
Figure 2-1 Stress distribution model for grouted bolts (*after* Xueyi, 1983)

$$\frac{d\tau_z}{dz} = \frac{d^2\sigma_z}{dz^2} = 0 \qquad\qquad (2\text{-}3)$$

The shear stress distribution is characterized by the division of the bolt into a pick-up length and an anchor length, on either side of the neutral point. This is justified mathematically by considering the equilibrium of the grouted bolt relative the surrounding rock. The pick-up length restrains the ground displacements towards the opening whereas the anchor length is restrained by the rock. The equilibrium of the bolt relative to the rock is thereby ensured as a result of the shear stresses acting in opposite directions along the pick-up length and anchor length, respectively. The relative displacement at the neutral point is essentially zero. Yu and Xian (1983) have independently investigated the interaction mechanisms of the fully grouted bolts and have provided further theoretical support for the above described model. The location of the neutral point along the bolt has been determined by equilibrium considerations, and it is given by:

$$\rho = \frac{L}{\ln\left[1+(\frac{L}{r_i})\right]} \qquad\qquad (2\text{-}4)$$

where L is bolt length and r_i is opening radius. According to observations, it was seen that $\rho \sim 0.45L+r_i$ or $L \sim (20\text{-}30)\ d$.

For a axi-symmetrical problem and considering identical bolt with equal spacing along the opening axis and around the circumference, the tangential bolt spacing around the opening is defined by the product of the opening radius and the angle between two adjacent bolts (i.e. $S_T = r_i\ \theta$) see Figure 2-2.

2.3 Influence of bolting on strength parameters and bolt density parameter

The equilibrium of an element near an unsupported opening in accordance with theory of elasticity (Figure 2-2) can be represented by:

$$\frac{d\sigma_r}{dr} + \frac{\sigma_r - \sigma_\theta}{r} = 0 \tag{2-5}$$

Combination of the non-linear Hoek & Brown post-failure criterion (Equation 1-15), the Equation 2-5 leads to the following, referred to as the unsupported tunnel:

$$\frac{d\sigma_r}{dr} - \frac{\sigma'_{ci}(m_b{}'\frac{\sigma_r}{\sigma'_{ci}} + s')^{a'}}{r} = 0 \tag{2-6}$$

In a bolted element (Figure 2-2d), the additional radial force due to shear stresses along the bolt is assumed to be given by the following expression (Indraratna, 1987):

$$\Delta\tau = \pi \cdot d \cdot \sigma_\theta \cdot \lambda \cdot dr \tag{2-7}$$

The equilibrium condition for this segment of longitudinal length S_L can be represented by

$$\frac{d\sigma_r}{dr} - \frac{1}{r}\sigma'_{ci}(1+\beta)\left[m'_b(1+\beta)\frac{\sigma_r}{\sigma'_{ci}(1+\beta)} + s'(1+\beta) \right]^a = 0 \tag{2-8}$$

where the bolt density parameter can be defined as:

$$\beta = \frac{\pi d \lambda}{S_L \theta} = \frac{\pi d \lambda r_i}{S_L S_T}$$ (2-9)
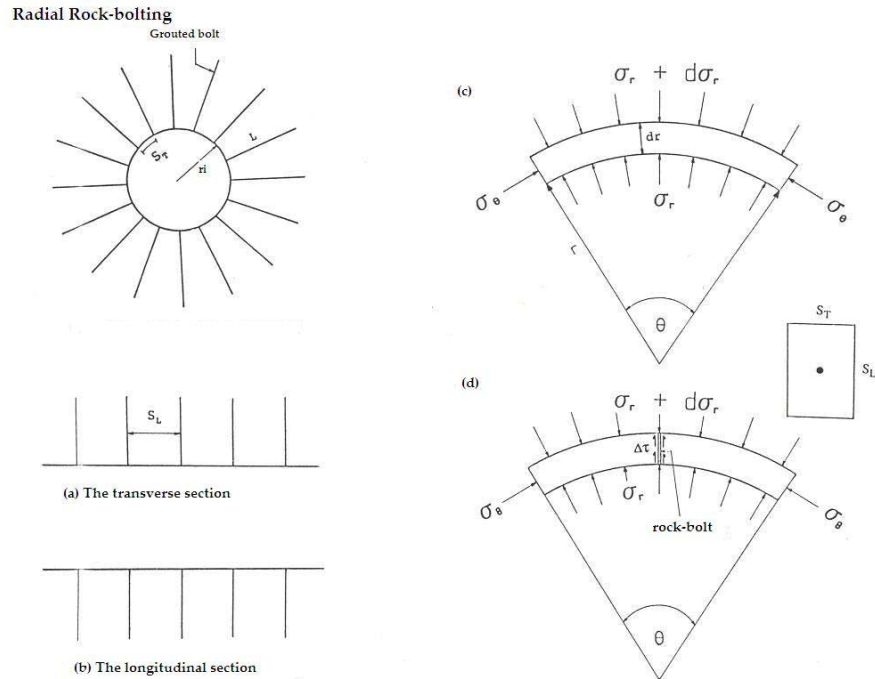
Figure 2-2 Fully reinforced circular excavation and equilibrium considerations for bolt-ground interaction

where d is the bolt diameter, r_i is the tunnel radius, λ is the friction factor for bolt / grout interface, and S_L and S_T are the longitudinal and transversal bolt spacings, respectively. As apparent, the bolt density parameter (β) is dimensionless. It reflects the relative density of bolts with respect to the opening perimeter and takes into consideration the shear stresses on the bolt surface, which oppose the rock mass displacements near the opening wall. The magnitude of β can be increased by:

    I.   Decreasing the bolt spacing

    II.   Increasing the bolt surface area

    III.   Increasing the roughness of bolt surface

In practice, the value of β varies between 0.05 and 0.20 for most cases. For openings excavated in poor rock mass such at the Enasan tunnel, analyzed by Indraratna & Kaiser (1990a) very high values for β (in excess of 0.4) were reached by very intensive bolting patterns.

The friction factor, λ, is analogous to the coefficient of friction. It relates the mean mobilized shear stress to the stress applied normal to the bolt surface. The magnitude of λ for smooth rebars falls in the range *tan (φ_g/2) < λ < tan ($2\varphi_g$/3)* and for shaped rebars approaches tanφ_g, depending on the degree of adhesion (bond strength) at the bolt/grout interface. The friction angle of a hardened grout (cement or resin) is comparable to that of most intact rock. The ratios β/λ for many case histories determined by Indraratna & Kaiser (1990a) indicates that the β/λ varies between 0.12 and 0.41 in a normal manner.

The bolt length, another important parameter for controlling displacements, is not included in the bolt density parameter because the effect of a bolt depends on its length relative to the radius of the yield zone. The shear stress distribution and, hence, the location of the neutral point are directly related to the bolt length, the extent of the plastic zone and the strength reduction in this zone. As will be shown later, the extent of the yield zone and the opening wall displacements can be effectively reduced by increasing the bolt length.

2.4 Concept of equivalent material approach (equivalent strength parameters)

By embedding the grouted rock-bolts in disturbed zone (yielded zone) around the tunnel, already characterized in terms of residual (post-peak) strength parameters, the strength parameters (Hoek & Brown constants) of the disturbed rock mass will then be improved. In other words, grouted rock-bolts create a zone of improved, reinforced rock in the region defined by the pick-up length of the bolts. Within this zone, the strength parameters of yielded rock mass are increased as schematically shown in the Figure 2-4.

Introducing the bolt density parameter (β), the equivalent strength parameter can be hypothesized as:

$$m_b^* = (1+\beta)m_b'$$

$$s^* = (1+\beta)s' \tag{2-10}$$

$$\sigma_{ci}^* = (1+\beta)\sigma_{ci}'$$

The definition of above equations is graphically illustrated in Figure 2-5 to Figure 2-7. The Equation 2-8 for bolted structure can be simplified as follows:

$$\frac{d\sigma_r}{dr} - \frac{\sigma_{ci}^*(m_b^* \dfrac{\sigma_r}{\sigma_{ci}^*} + s^*)^a}{r} = 0 \tag{2-11}$$

Comparison of this equation with Equation 1-27 for the unsupported case indicates that both equations have the same algebraic arrangement.

It is worth noting that the coefficient *a* for the reinforced tunnel is assumed to not be affected by the (*β*), rather it keeps its original value of 0.5 (i.e. $a^* = a$).

2.5 Rock stabilization through effective material strength parameters

As mentioned before, the strength parameters of rock mass (*c* and *φ* in Mohr-Coulomb criterion and *m, s, a* and *σ_{ci}* in Hoek-Brown criterion) in yielding zone around the opening (or ahead of the face) may be assumed to be degrade from peak value to residual values identified with the primed superscript in the Figure 2-8.

Conversely, the Mohr envelope of the broken material may be raised up by improving its strength parameters (*c** and *φ** in Mohr-Coulomb criterion and *m*, s*,* and *σ_{ci}** in Hoek-Brown criterion) by application of a radial, confining pressure through the use of grouted bolts.

The development of load on a grouted bolt has the effect of providing additional confinement (increased radial stress) in the yielded zone. As a result the tangential stress at the same point is increased more than proportionately. The original failure envelope is thereby shifted upwards, indicating an improvement of the strength parameters as represented by the Mohr diagram in Figure 2-8. This enables the rock mass to behave as a stronger material leading to a corresponding reduction in opening convergence at a given field stress.

The following expression has been introduced in the literature to show the effect of the rock bolting on improving of the yielding zone around the tunnel in terms of effective cohesion (Grasso et al. 1989, Pelizza et al. 2006).

$$c^* = c + \frac{1 + \sin \varphi}{2 \cos \varphi} \cdot \Delta \sigma_3 \qquad (2\text{-}12)$$

where $\Delta \sigma_3$ is the confinement produced by the action of the grouted bolts:

$$\Delta \sigma_3 = \frac{T_m}{S_T \cdot S_L} \qquad (2\text{-}13)$$

where T_m is the mean force along each bolt, S_T and S_L are transversal and longitudinal spacing of the bolting pattern.

Grouted bolts themselves are not considered to establish any radial support pressure, P_i, on the rock surface, so equilibrium for the ground reaction curve is

reached as for unsupported rock when $P_i=0$. The principal effect of grouted bolts, compared to the unsupported rock mass, is that the stability of rock mass is improved as the bolts through tension load influence the strength of the rock mass and the volume expansion at failure. Consequently, owing to the fact that fully grouted bolts effectively improve the apparent strength of the rock mass, the behaviour of the reinforced opening can be ideally represented by a shift of the ground convergence curve. The vertical axis of the ground convergence curve (Figure 2-3) represents the fictitious radial stress (σ_s) required at the opening boundary to prevent further convergence. The horizontal axis represents the opening convergence at the opening wall (u_{ri}). The ground convergence curves are identical at every point along the opening boundary for the condition of axisymmetric yielding under hydrostatic field stress.

The response of an unsupported opening in yielding rock is given by curve A. curve B represents an imaginary ground convergence curve of the opening, where bolts would have been installed before any displacements could have occurred. In reality, an initial displacement (u_o) of the opening wall occurs prior to the installation and subsequent activation of the grouted bolts. The magnitude of convergence after bolting is dependent on the apparent stiffness of the bolt/ground composite, and is reflected by a shift of the ground convergence curve from curve A to curve C, as a result of the reduced yield zone. An example of ground reaction curve of a reinforced tunnel will be presented in the following sections. In contrast to fully grouted bolts, pre-tensioned mechanical bolts provide direct radial pressure (active support) against the opening wall, but do not become an integral part of the deforming rock mass. Consequently, their performance is best represented by a support confinement curve with a specific stiffness and its interaction with the original ground convergence curve.
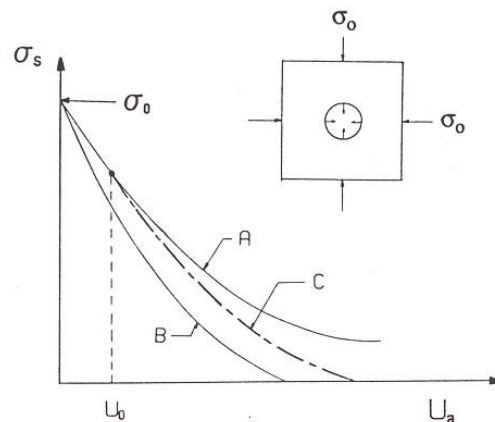
Figure 2-3 The effect of grouted bolts on the Ground Reaction Curve

a) Plastic zone induced around the unsupported tunnel

Residual (Post-peak) strength parametes mb', s', σ'ci

b) Grouted rock-bolts are installed in the already induced yielded zone around the tunnel

a) Induced plastic zone + grouted rock bolt can be considered as the Equivalent Plastic Zone

Equivalent strength parametes mb*, s*, σ*ci
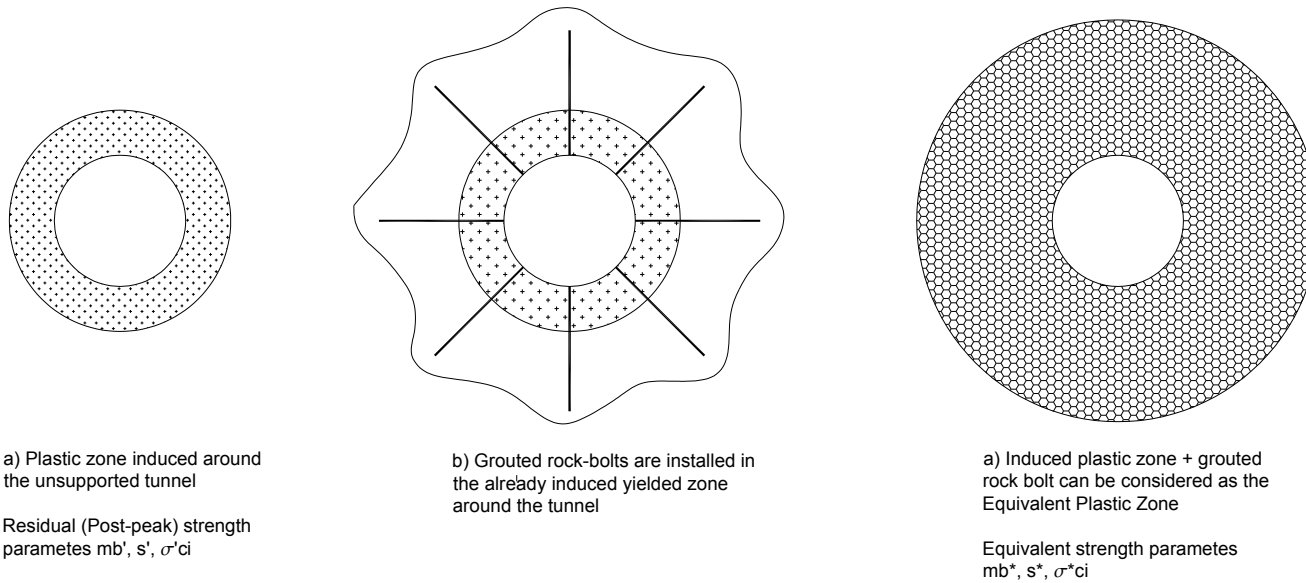
Figure 2-4 Creation of the Equivalent Plastic Zone around the circular tunnel reinforced by grouted rock-bolts
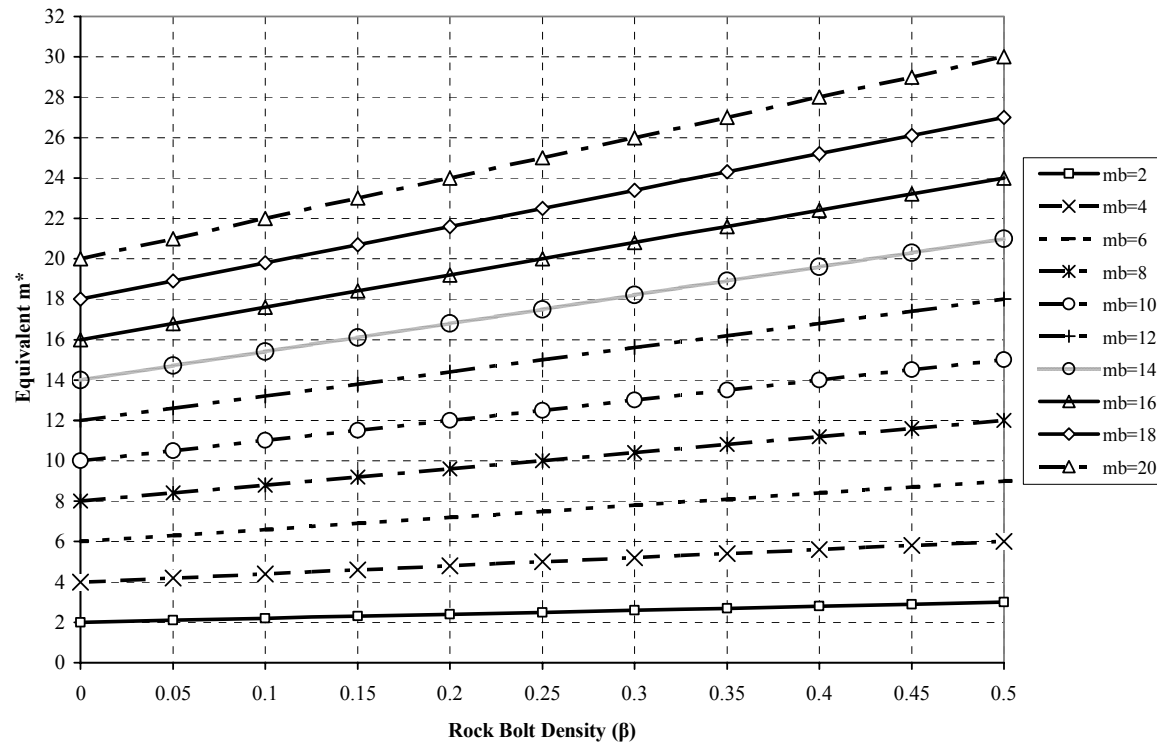
Figure 2-5 Variation of the Equivalent strength parameter "m*" of Hoek & Brown failure criterion with β
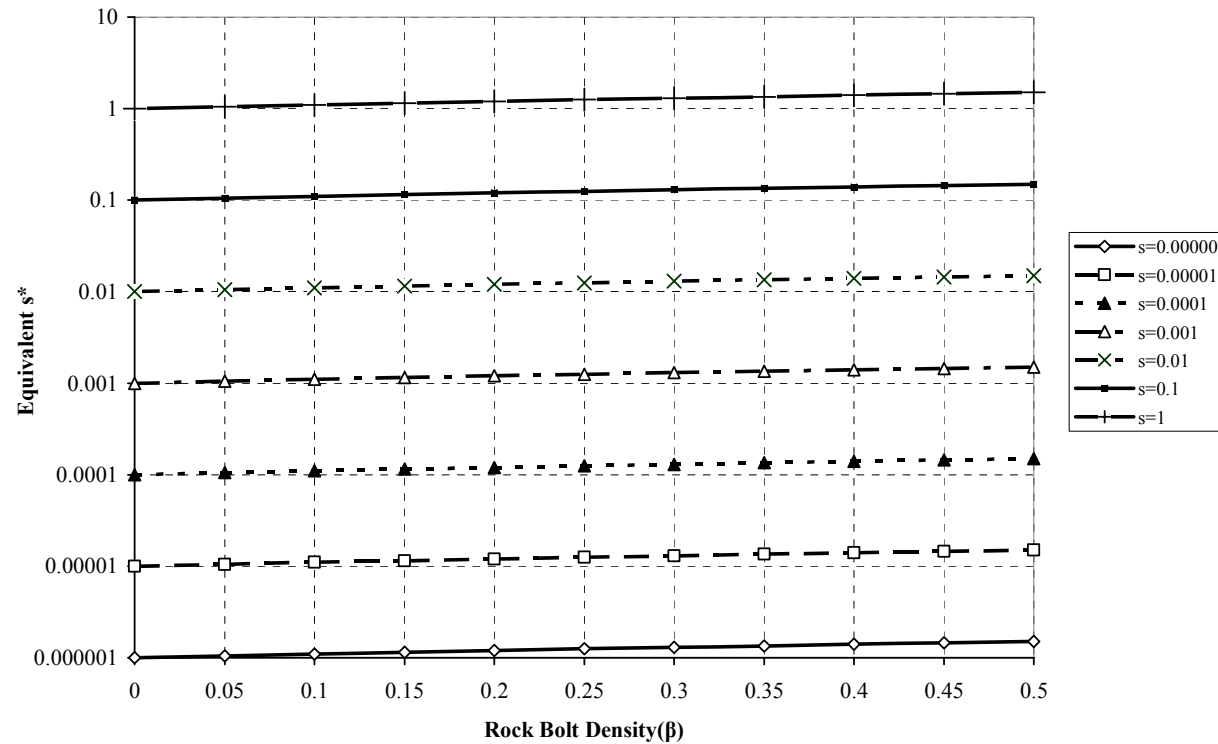
Figure 2-6 Variation of the Equivalent strength parameter "s*" of Hoek & Brown failure criterion with β
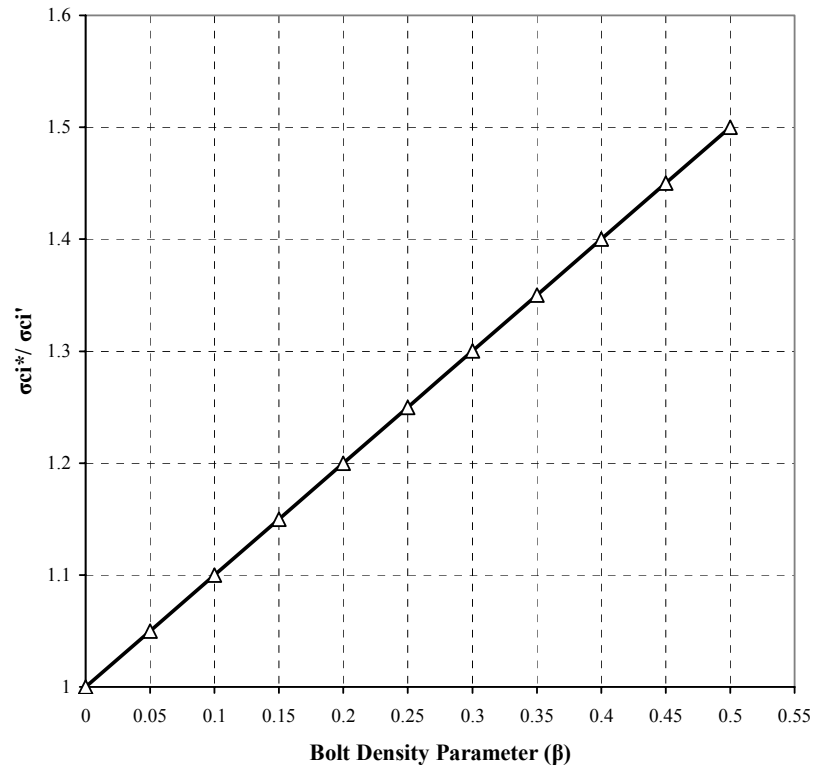
Figure 2-7 Variation of the Equivalent Compressive Strength with β
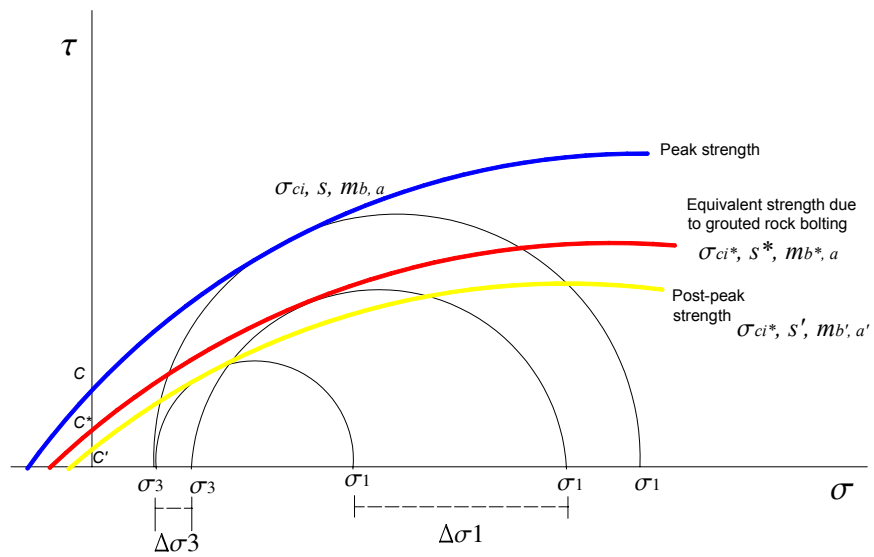
Figure 2-8 Increase of strength parameters by reinforcing the ground

2.6   Influence of bolt length on tunnel wall stability

One other important parameter for controlling displacement, i. e. the bolt length, is not included in the bolt density parameter because the effect of a bolt depends on its length relative to the radius of the yield zone. The shear stress distribution and, hence, the location of the neutral point are directly related to the bolt length, the extent of the plastic zone and the strength reduction in this zone. As it will be shown later, the extent of the yield zone and the tunnel wall displacement (convergence) can be effectively reduced by increasing the bolt length.

2.7   Concept of equivalent plastic zone

Grouted bolting is capable of improving the weakened or loosened zone by increasing its apparent strength in terms of Hoek & Brown constants $(m_b, s, a,$ and σ_{ci}) as schematically represented in Figure 2-4. The extent of the plastic zone is directly related to this rock mass properties and any improvement of the rock strength must reduce the extent of the zone of overstressed rock, if the bolts are installed soon after excavation close to the face. Consequently, the plastic zone of a bolted opening is smaller than that of an unsupported opening in the same ground. This zone is called "**Equivalent Plastic Zone**" because it is the yield zone in a material of improved properties simulating a behaviour equivalent to the bolted rock mass. In other words, EPZ consists of a material with improved strength properties, representing the yielded, reinforced rock mass. A reduction of the apparent plastic zone, in turn, curtails opening wall displacement. The extent of the plastic zone is influenced by the mechanical parameters (Hoek & Brown constants) and is independent of the elastic parameters E and v. The following factors directly affect the radius r_e^* of the equivalent plastic zone:

       I.   Bolt density parameter, β

      II. Bolt length, L_b

     III. Radius of the neutral point of the bolt , ρ

     IV. Opening radius, r_i

     V.   Field stress, P_o

The determination of the equivalent plastic zone EPZ radius, r_e^*, must be divided into three categories depending on the location of the interface between the elastic rock and the equivalent plastic zone relative to the neutral point and the bolt length. These three categories are diagrammatically illustrated in Figure 2-9:

- $r_e^* < \rho < (r_i + L)$ minimal yielding
- $\rho < r_e^* < (r_i + L)$ major yielding
- $r_e^* > (r_i + L)$ excessive yielding

46

2.7.1   Determination of the Equivalent Plastic Zone Category I

The condition of minimal yielding "$r_e^* < \rho < (r_i + L_b)$" occurs either at relatively small field stresses or when the bolts are excessively long. In this case, the extent of the plastic zone is confined within the pick-up length of the bolt. In addition, four distinct zones can be identified by the location of the plastic zone corresponding to the neutral point and the bolt ends.

L_b

Minimal yielding

$r_e^* < \rho < (r_i + L_b)$

r_i

r_e^*

τ_z

ρ

Major yielding

$\rho < r_e^* < (r_i + L_b)$

Excessive yielding

$r_e^* > (r_i + L_b)$
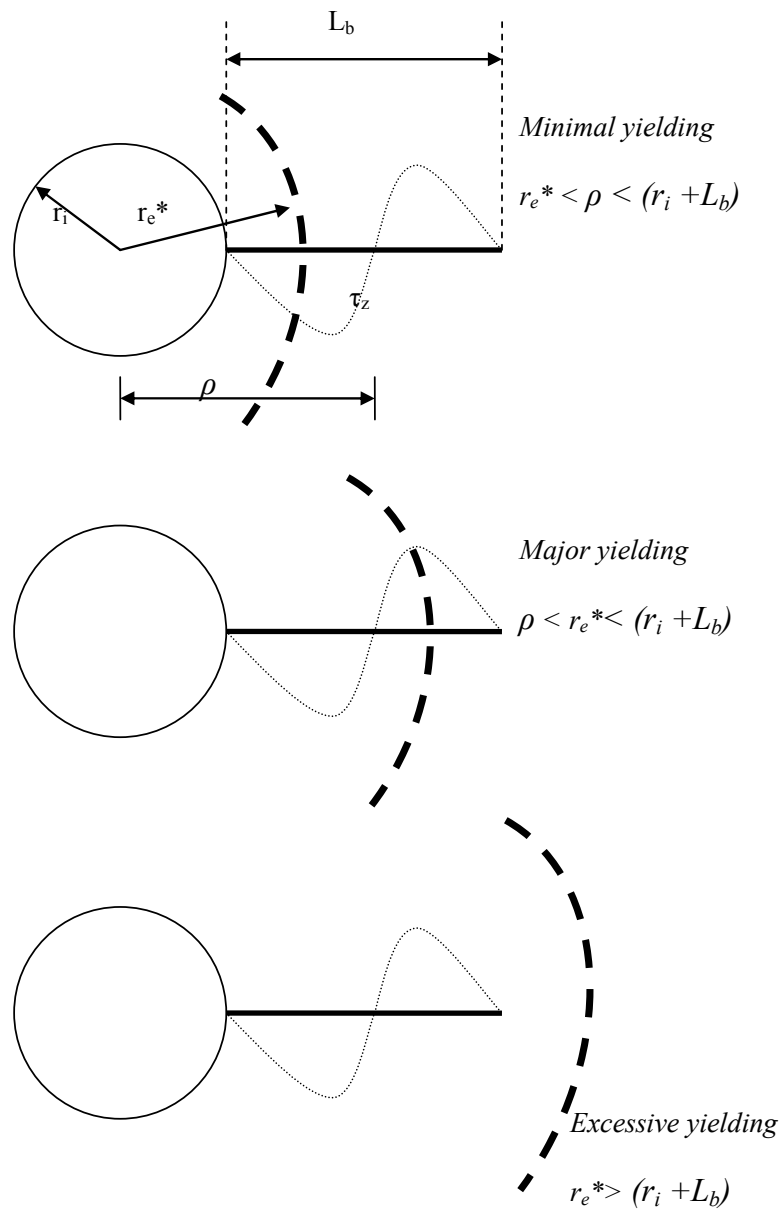
Figure 2-9 Categorization of the extent of the yielding (plastic zone)

2.7.1.1   Zone 1 : $r_i < r < r_e*$

In this region of the pick-up length, the ground displacements toward the opening are resisted by positive shear stress. The equivalent stress field in this zone is   represented by:

$$\sigma_r = \frac{\Gamma^* - s^*}{\dfrac{m_b^*}{\sigma_{ci}^*}} \qquad (2\text{-}14)$$

$$\Gamma^* = \left[s^{*1-a} - m_b^*(a-1)\ln\left(\frac{r}{r_i}\right) \right]^{\frac{1}{1-a}} \qquad (2\text{-}15)$$

$$\sigma_\theta = \sigma_r + \sigma_{ci}^*\left(m_b^* \frac{\sigma_r}{\sigma_{ci}^*} + s^* \right)^a \qquad (2\text{-}16)$$

where: $m_b^* = (1+\beta)m_b'$, $s^* = (1+\beta)s'$, $\sigma_{ci}^* = (1+\beta)\sigma_{ci}'$, $\sigma_{ci}' = S.\sigma_{ci}$

2.7.1.2   Zone 2 : $r_e* < r < \rho$

This part of the elastic zone is confined to the pick-up length of the bolt. The elastic stress fields in this zone are given by:

$$\sigma_r = P_o\left[1 - \left(\frac{r_e^*}{r}\right)^2 \right] + \sigma_{re}\left(\frac{r_e^*}{r}\right)^2 \qquad (2\text{-}17)$$

$$\sigma_\theta = P_o\left[1 + \left(\frac{r_e^*}{r}\right)^2 \right] - \sigma_{re}\left(\frac{r_e^*}{r}\right)^2 \qquad (2\text{-}18)$$

The peak tangential stress at the elasto-plastic interface for $S=1$ is given by the following condition:

$$\sigma_{\theta e} = \sigma_{re} + \sigma_{ci}^*\left(m_b^* \frac{\sigma_{re}}{\sigma_{ci}^*} + s^* \right)^a \qquad (2\text{-}19)$$

48

The radial stress at the elasto-plastic boundary σ_{re} is, therefore, derived by:

$$\sigma_{re} = \frac{\Delta^* - s^*}{\dfrac{m_b^*}{\sigma_{ci}^*}} \tag{2-20}$$

$$\Delta^* = \left[s^{*1-a} - m_b^*(a-1)\ln\left(\frac{r_e^*}{r_i}\right) \right]^{\frac{1}{1-a}} \tag{2-21}$$

2.7.1.3   Zone 3 : $\rho < r < (r_i + L_b)$

This part of the elastic zone is contained within the anchor length of the bolt. The radial and tangential stress fields are given by:

$$\sigma_r = P_o\left[1 - \left(\frac{\rho}{r}\right)^2\right] + \sigma_\rho\left(\frac{\rho}{r}\right)^2 \tag{2-22}$$

$$\sigma_\theta = P_o\left[1 + \left(\frac{\rho}{r}\right)^2\right] - \sigma_\rho\left(\frac{\rho}{r}\right)^2 \tag{2-23}$$

where

$$\sigma_\rho = P_o\left[1 - \left(\frac{r_e^*}{\rho}\right)^2\right] + \sigma_{re}\left(\frac{r_e^*}{\rho}\right)^2 \tag{2-24}$$

2.7.1.4   Zone 4 : $r > (r_i + L_b)$

This outermost elastic region, beyond the bolt, is in virgin rock and the elastic stresses are given by:

$$\sigma_r = P_o\left[1 - \left(\frac{r_i + L_b}{r}\right)^2\right] + \sigma_{L_b}\left(\frac{r_i + L_b}{r}\right)^2 \tag{2-25}$$

$$\sigma_\theta = P_o\left[1 + \left(\frac{r_i + L_b}{r}\right)^2\right] - \sigma_{L_b}\left(\frac{r_i + L_b}{r}\right)^2 \tag{2-26}$$

where

$$\sigma_{L_b} = P_o\left[1-\left(\frac{\rho}{r_i+L_b}\right)^2\right] + \sigma_\rho\left(\frac{\rho}{r_i+L_b}\right)^2 \tag{2-27}$$

The radial distance to the neutral point is given by Equation 2-4, as discussed earlier.

2.7.1.5 Equivalent Plastic Zone (EPZ)

At the elastic-plastic interface, the radial stress σ_{re} is obtained by Equations 2-20 and 2-21 through the assumption of continuity of radial stress. Equating Equations 1-40 and 2-20 and then solving provides the normalized radius of the equivalent plastic zone (EPZ):

$$\frac{r_e^*}{r_i} = e^Y \tag{2-28}$$

$$Y = \frac{s^{*\,1-a} - \left\{s^* + \frac{P_o m_b^*}{\sigma_{ci}^*} + \frac{m_b m_b^* \sigma_{ci}}{8\sigma_{ci}^*} - \frac{m_b^*}{8\sigma_{ci}^*}\left(16P_o m_b \sigma_{ci} + m_b^2 \sigma_{ci}^2 + 16\sigma_{ci}^2 s\right)^{\frac{1}{2}}\right\}^{1-a}}{m_b^*(a-1)}$$

It is obvious that as β tends to zero, the parameters m_b^*, s^*, and σ_{ci}^* approach m_b, s, and σ_{ci}. In other word, above equation becomes identical to that of unsupported case as Equation 1-43. Note that the equivalent value of a keeps its original value. Expressions for the Equivalent Plastic Zone radius can be derived for Categories (II) and (III) in the same manner. A summary is given below.

2.7.2   Determination of the Equivalent Plastic Zone Category II

The condition of major yielding, $\rho < r_i^* < (r_i+L_b)$, occurs when the extent of the plastic zone has propagated beyond the neutral point. In this situation, the plastic zone itself is divided by the neutral point into two zones. Consequently, only the plastic zone region that falls within the pick-up length of the bolt is effectively stabilized by the positive shear stresses. The Equivalent Plastic Zone radius is given by:

$$\frac{r_e^*}{r_i} = e^J \cdot e^h = e^{(J+h)} \tag{2-29}$$

50

where

$$J = \frac{(m_{b1}\sigma_\rho + \sigma_{ci1}s_1)^{1-a'} - \left[s_1\sigma_{ci1} + P_o m_{b1} + \frac{m_b m_{b1}\sigma_{ci}}{8} - \frac{m_{b1}}{8}(16P_o m_b \sigma_{ci} + m_b^2 \sigma_{ci}^2 + 16\sigma_{ci}^2 s)^{\frac{1}{2}} \right]^{1-a'}}{m_{b1}(a'-1)\sigma_{ci1}^{(1-a')}}$$

$$h = \frac{s^{*^{1-a}} - \Gamma^{*^{1-a}}}{m_b^*(a-1)}$$

$$\sigma_\rho = \frac{\Gamma^* - s^*}{\frac{m_b^*}{\sigma_{ci}^*}}$$

$$\Gamma^* = \left[s^{*^{1-a}} - m_b^*(a-1)\ln\left(\frac{\rho}{r_i}\right) \right]^{\frac{1}{1-a}}$$

$$m_{b1} = m_b'(1-\beta) \quad s_1 = s'(1-\beta) \quad \sigma_{ci1} = \sigma_{ci}'(1-\beta)$$

2.7.3 Determination of the Equivalent Plastic Zone Category III

The condition of excessive yielding, $r_e^* > (r_i + L_b)$, occurs either due to large *in-situ* stress in relatively poor rock or as a result of inadequate bolt length. In this situation, the bolt is completely embedded in the yielded rock and no anchorage is provided from the outer elastic zone. In this case the radius of the Equivalent Plastic Zone is obtained by:

$$\frac{r_e^*}{r_i} = e^q \cdot e^h \cdot e^t = e^{(q+h+t)} \tag{2-30}$$

$$q = \frac{(m_b'\sigma_L + \sigma_{ci}'s')^{1-a'} - \left[s'\sigma_{ci}' + P_o m_b' + \frac{m_b m_b'\sigma_{ci}}{8} - \frac{m_b'}{8}(16P_o m_b \sigma_{ci} + m_b^2 \sigma_{ci}^2 + 16\sigma_{ci}^2 s)^{\frac{1}{2}} \right]^{1-a'}}{m_b'(a'-1)\sigma_{ci}'^{(1-a')}}$$

$$h = \frac{s^{*^{1-a}} - \Gamma^{*^{1-a}}}{m_b^*(a-1)}$$

$$t = \frac{(m_{b1}\sigma_\rho + s_1\sigma_{ci1})^{1-a'} - (m_{b1}\sigma_L + s_1\sigma_{ci1})^{1-a'}}{m_{b1}(a'-1)\sigma_{ci1}^{1-a'}}$$

51

$$\sigma_L = \frac{\dfrac{\xi}{\sigma_{ci1}} - s_1}{\dfrac{m_{b1}}{\sigma_{ci1}}}$$

$$\xi = \left[(m_{b1}\sigma_\rho + \sigma_{ci1}s_1)^{1-a'} - m_{b1}(a'-1)\sigma_{ci1}^{1-a'} \ln\left(\frac{r_i + L_b}{\rho}\right) \right]^{\frac{1}{1-a'}}$$

$$\sigma_\rho = \frac{\Gamma^* - s^*}{\dfrac{m_b^*}{\sigma_{ci}^*}}$$

$$\Gamma^* = \left[s^{*1-a} - m_b^*(a-1)\ln\left(\frac{\rho}{r_i}\right) \right]^{\frac{1}{1-a}}$$

$$m_{b1} = m_b'(1-\beta) \quad s_1 = s'(1-\beta) \quad \sigma_{ci1} = \sigma_{ci}'(1-\beta)$$

Having determined the Equivalent Plastic Zone r_e^* with respect to its category (categories I to III), the ultimate tunnel convergence can be obtained by:

$$\frac{u_{ri}^*}{r_i} = \frac{1}{2G}\left[M\sigma_{ci}\left(\frac{r_e^*}{r_i}\right)^{(1+N_\psi)} + \frac{1}{r_i^{(1+N_\psi)}}\sigma_{ci}'(1-\nu)(2 + a'm_b')\int_{r_i}^{r_e} r^{N_\psi-1}\Gamma^{a'}dr \right] \quad (2\text{-}31)$$

$$\Gamma = \left[s'^{1-a'} - m_b'(a'-1)\ln\left(\frac{r}{r_i}\right) \right]^{\frac{1}{1-a'}}$$

$$M = \frac{1}{2}\left[\left(\frac{m_b}{4}\right)^2 + m_b\frac{P_o}{\sigma_{ci}} + s \right]^{\frac{1}{2}} - \frac{m_b}{8}$$

The formulations of elasto-plastic solution for grouted bolt design are presented in spreadsheet presented in the Appendix B.

2.8 Practical application of the proposed elasto-plastic solution

The following example, posed by Hoek & Brown (1980) and Carranza-Torres (2004), is intended to illustrate the practical application of the proposed

approach in determining the elasto-plastic response of an opening. Two cases are considered, one for an unsupported tunnel, the other for a tunnel reinforced by grouted bolts, both for a rock mass of known properties outlined in the Table 2-1. The solution of this example in the form of spreadsheet is given in Appendix B.

Calculated radial and tangential stresses are shown in the Figure 2-10, indicating that the radius of plastic zone is 5.09 m. The maximum displacement of the tunnel surface is found to be 30.7 mm as illustrated in Figure 2-13. The Ground Reaction Curve, often being used in the rock-support interaction analysis, is depicted in Figure 2-11.

The effect of the grouted bolts can be best described with reference to the Figure 2-12, Figure 2-13, and Figure 2-14. As can be seen from Figure 2-12, the additional radial stress can be attributed as previously presented in Figure 2-8. Also it can be observed that the radius of the plastic zone decreases from 5m to 4.6m while a convergence reduction by 20 % is recorded as referred to Figure 2-13.

Table 2-1 Input parameters used in the practical example

Rock mass properties		Grouted bolt specifications	
ri(m)	2	λ	0.6
Po (MPa)	15	d (mm)	32.00
E(Gpa)	5.7	Cb (kN)	280.00
ν	0.3	St (m)	1.00
σci	30	Sl (m)	1.00
ψ	0	Lb (m)	3.00
mb	1.7	ρ(m)	3.27
s	3.90E-03	β	0.121
mb'	0.85	mb*	0.953
s'	1.90E-03	σci*	30.257
a	0.5	s*	2.129E-03
S	1		
σci'	27		
r(m)	2		
a'	0.5		
Nψ	1		
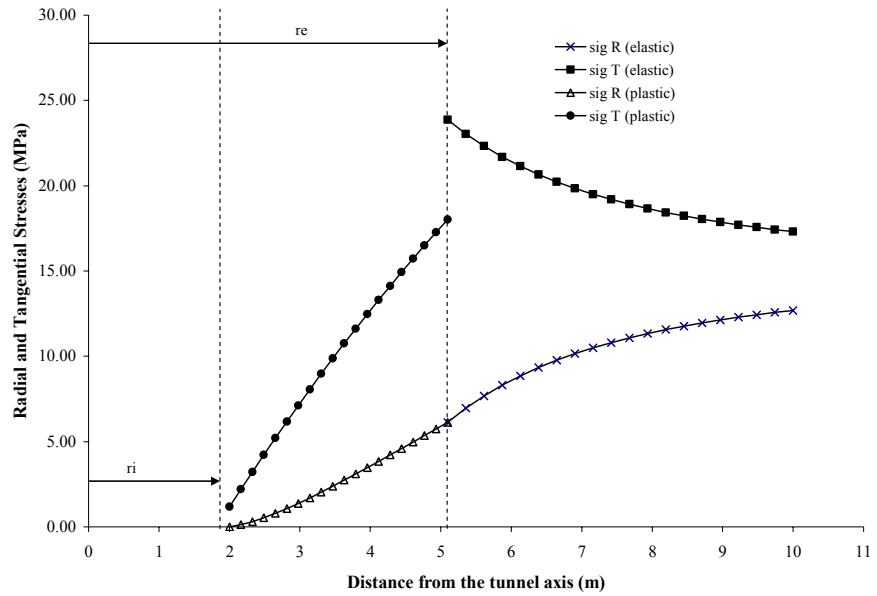
Figure 2-10 Stress field around the unsupported tunnel surface
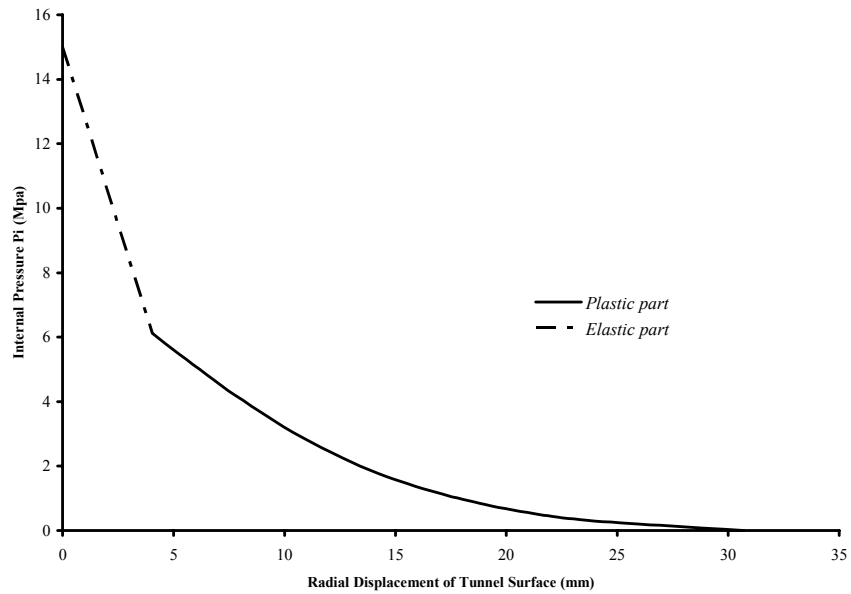
Figure 2-11 Ground Reaction Curve (GRC) of unsupported tunnel (natural ground) based on proposed elastic- plastic model
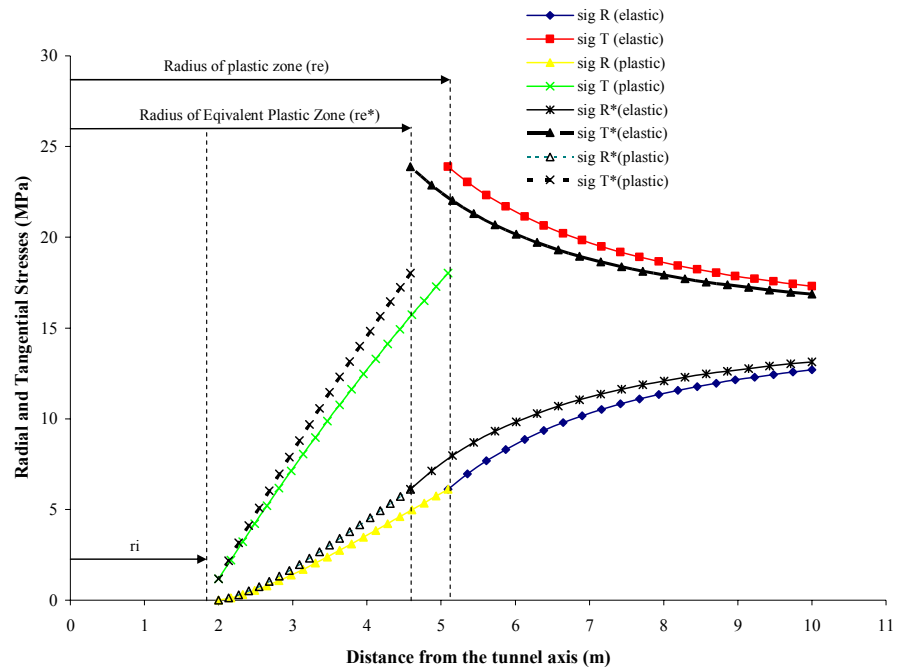
Figure 2-12 Radial and tangential stresses field near the reinforced tunnel
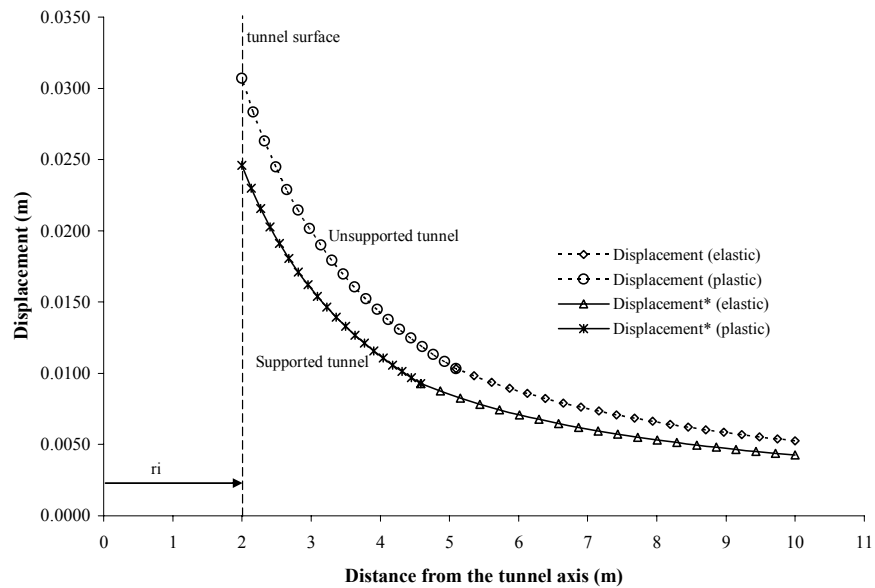
Figure 2-13 Comparison of the tunnel surface displacement for both unsupported and reinforced tunnel cases
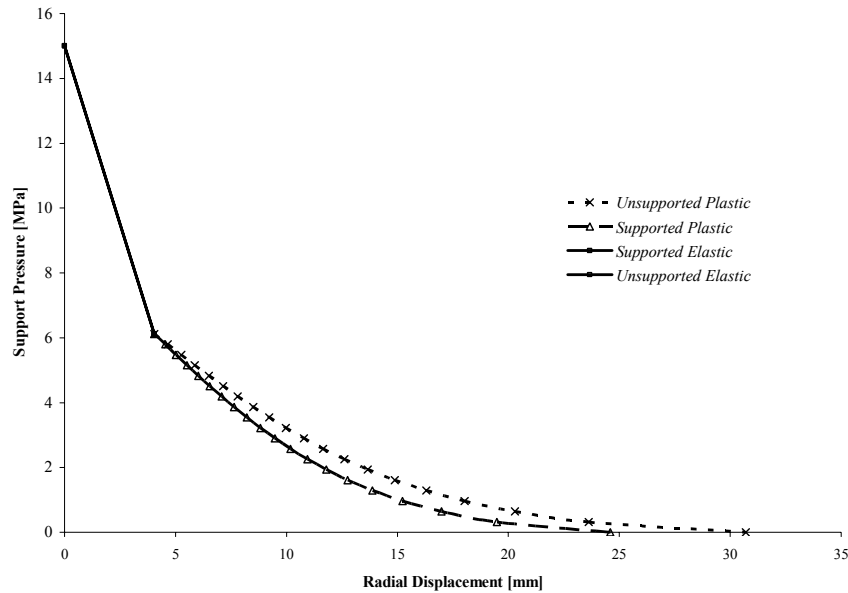
Figure 2-14 Ground Reaction Curve (GRC) with and without grouted bolts based on proposed elasto-plastic model

A helpful distinction to notice is that unlike the mechanical rock bolts which can be modelled through the Support Reaction Curve, the grouted bolts effect can be best investigated by reinforced ground reaction curve. This is due to the fact that in contrast to fully grouted bolts, mechanical bolts provide direct radial pressure against the tunnel wall, but do not become an integral part of the deformed rock mass. Consequently, their performance is appropriately represented by a support confinement curve with specific stiffness and its interaction with the original ground reaction curve. In brief, the effect of grouted bolts on ground improvement in terms of its elasto-plastic response is represented by GRC as shown in the Figure 2-14 for this example.

2.9 The effect of the bolt density on stresses and displacement field

The following example will depicts the influence of the bolt density on stresses and displacements field around a reinforced tunnel by grouted bolts. The input parameters of the example are given in the Table 2-2.

The predicted stress and displacement fields for this tunnel, reinforced with 32 mm grouted bolts and subjected to a far field stress of 15 MPa are presented in Figure 2-15 and Figure 2-16, respectively. Different bolt patterns ($\beta=0$ to $\beta=0.3$) are taken into account for comparison.

Table 2-2 Input parameters used in this analysis

r_i (m)	2
Po (MPa)	15
E (Gpa)	5.7
ν	0.3
σ_{ci} (MPa)	30
ψ	0
m_b	1.7
s	3.90E-03
m_b'	0.85
s'	1.90E-03
a	0.6
S	1
$\sigma ci'$ (MPa)	25
r (m)	2
a'	0.6
Nψ	1

It can be seen from Figure 2-15 that as the bolt density parameter β increases, the radial and tangential stress fields approach those predicted for non-yielding, elastic rock, and the radius of equivalent plastic zone (r_e*) approaches the tunnel radius. Further away from the tunnel, the stresses field approaches the far field stress.

For displacement field as shown in the Figure 2-16, as β increases, the displacement approaches the elastic solution. As distance from the tunnel wall increases, the effect of bolting diminishes rapidly and the far field conditions are obtained. It is evident that the maximum decrease in strains and radial displacements occurs at the tunnel wall. Hence, the tunnel wall convergence can be well-considered as the most appropriate parameter for a displacement control design approach.

2.10 Normalized convergence ratio

The total displacement (convergence) of a reinforced tunnel u_{ri}* is a function of the rock mass, the field stress level and the reinforcement configuration. On the other side, the convergence of a reinforced tunnel can be presented by the dimensionless ratio u_{ri}*$/u_{ri}$, where u_{ri}* and u_{ri} are the total convergence of the reinforced and unsupported opening respectively at the same stress level. The total opening convergence includes both the elastic and plastic displacements. For a given field stress, u_{ri}* is less than u_{ri} but it approaches u_{ri} when the bolt density (β) or the bolt length (L_b) tends to zero.
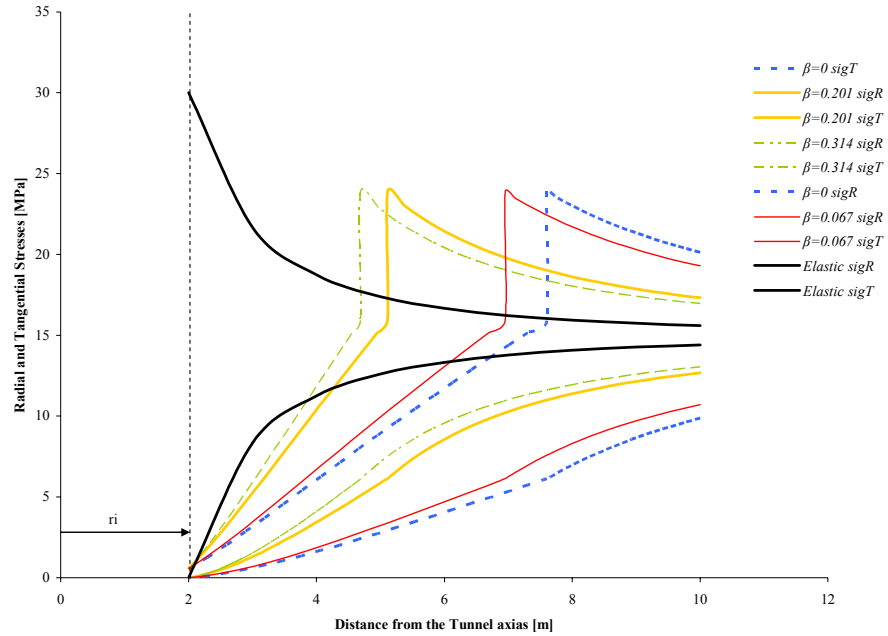
Figure 2-15 Stress field near the tunnel for different value of the bolt density parameter β
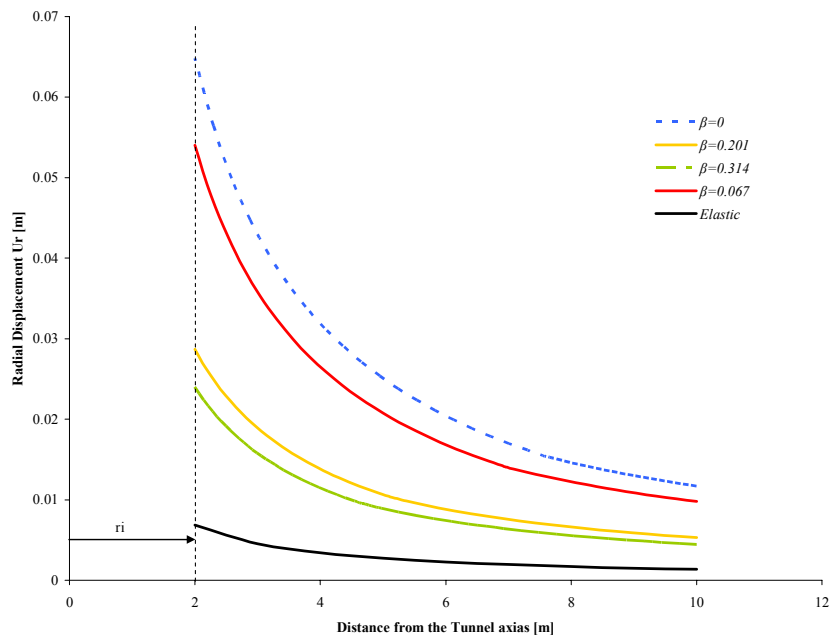
Figure 2-16 Displacement field near the tunnel for different value of the bolt density parameter β

The normalized convergence ratio decreases as the intensity of bolting increases. It obtains a minimum value when u_{ri}^* tends to u_e, the elastic portion of the total convergence. The latter condition may be approached at every intensive bolt densities such as $\beta > 0.30$, which is not only rare in practice but is economically unattractive. The convergence ratio is particularly useful in the design of grouted bolts, since it reflects the reduction in convergence that can be achieved by a given bolting pattern.

An important characteristic of the convergence ratio is that it is insensitive to moderate changes of the deformation and strength parameters. For instance, a change in Young's modulus affects both u_{ri}^* and u_{ri} equally, hence the ratio u_{ri}^*/u_{ri} remains unaltered. The latter characteristic of the normalized convergence ratio makes its use in design even more reliable, since the variation of *in-situ* geotechnical parameters can be tolerated without any significant error.

2.10.1 Normalized convergence ratio as a design aid

The normalized convergence ratio u_{ri}^*/u_{ri} is relatively insensitive to moderate change of the fundamental similitude parameters (m ,s ,σ_{ci}, E, v , etc.) for a given reinforcement configuration (β, L_b).

Figure 2-17 depicts the predicted results of analytical model for an example with various bolt pattern ($L_b / r_i = 1$) at applied field stress levels between 2 and 16 MPa. The obtained normalized convergence ratio u_{ri}^*/u_{ri} is plotted for these stress levels and five bolt density parameters β. u_{ri}^* and u_{ri} are the total convergence of the reinforced and unsupported tunnel, respectively.

The normalized convergence ratio decreases as β increases (i.e., the tunnel convergence reduction is almost proportional to the bolt density). It can be understood that the normalized convergence ratio is independent of the elastic constants and is insensitive to moderate change of the uniaxial compressive strength and Hoek & Brown strength parameters for a given configuration of reinforcement. Therefore, the normalized convergence ratio is applicable for design, even if the material properties cannot be clearly defined or if the in situ stress cannot be accurately estimated. It is believed that the relationship illustrated in Figure 2-17 for a given bolt length may be used for design purposes.

For instance, for a tunnel of 5 m diameter excavated in a relatively poor rock mass (in a field stress of 10 MPa, i.e. 400 to 450 m deep) with 2 m long grouted bolts ($Lb / r_i = 0.8$), the tunnel convergence (wall displacements) would be reduced by 33 % for a bolt density β of 0.265. This could be achieved by installing 45 mm shaped rebars (like self drilling anchors MAI-bolts $\lambda=0.6$) with a spacing of 0.8m x 0.8m.

ri(m)= 2
E(Gpa) =4,7
ν = 0,25
σci =40
ψ= 0
mb =1,4
s =2,20E-03
mb' =1
s' =1,60E-03
a =0,5
S =1
σci' =30
r(m) =2
a' =0,52
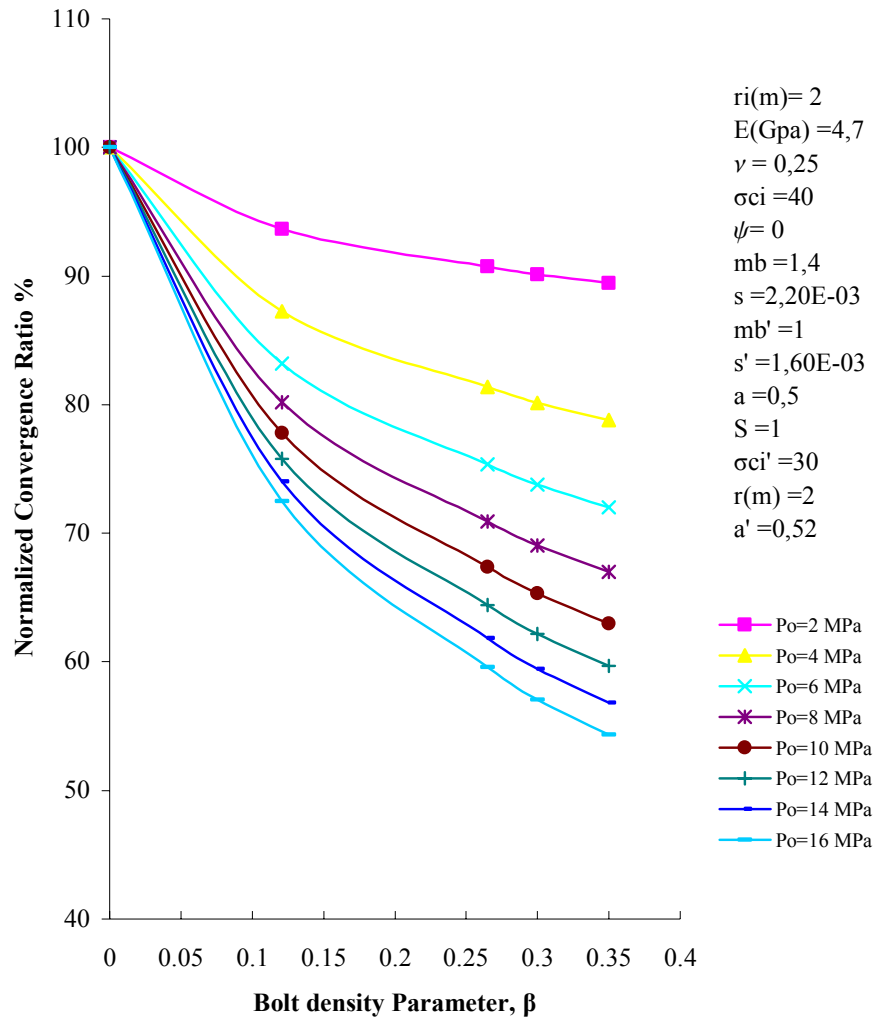
Figure 2-17 Variation of tunnel convergence with bolt density parameter for 2 m long grouted bolt

2.11 Influence of grouted bolts on tunnel stability

The radial strains and displacements at the tunnel wall are the most fundamental quantities required to evaluate the stability of a tunnel opening. In the field they are not only feasible to measure but are also generally reliable. The radial convergence of the reinforced opening wall can be predicted from the following equations, once the magnitude of r_e^* has been determined for the respective categories I to III as specified in the section 2.7.

$$\frac{u_{ri}^*}{r_i} = \frac{1}{2G}\left[M\sigma_{ci}\left(\frac{r_e^*}{r_i}\right)^{(1+N_\psi)} + \frac{1}{r_i^{(1+N_\psi)}}\sigma_{ci}'(1-\nu)(2+a'm_b')\int_{r_i}^{r_e} r^{N_\psi-1}\Gamma^{a'} dr \right] \quad (2-31)$$

$$\Gamma = \left[s'^{1-a'} - m_b'(a'-1)\ln\left(\frac{r}{r_i}\right) \right]^{\frac{1}{1-a'}}$$

$$M = \frac{1}{2}\left[\left(\frac{m_b}{4}\right)^2 + m_b\frac{P_o}{\sigma_{ci}} + s \right]^{\frac{1}{2}} - \frac{m_b}{8}$$

Figure 2-18 illustrates the variation of the predicted convergence of a case example for different bolt pattern obtained by the proposed analytical model. The applied far field stress ranges between 0 and 16 MPa. As the bolt density increases, the displacement of the reinforced tunnel surface ($u_{ri}*$) decreases and varies between the upper and lower bounds of the unsupported tunnel displacement (u_{ri} dashed line A) and the response of an opening in linear elastic rock (u_e dashed line F). For reinforced tunnel, a sudden increase in convergence (shift to the right as shown in Figure 2-18) occurs for β =0.35-0.121 at Po > 12 MPa. This transition takes place when all bolts become completely embedded in the plastic zone. When Category III: $r_e^*>(r_i +L)$ is reached.

2.12 Use of displacement control (convergence reduction) approach for design

The following example enlightens the use of the displacement control (convergence reduction) approach for design of grouted bolts. Consider a tunnel of 3 m radius excavated at a depth of 150 m in a relatively weak sedimentary rock mass with the representative material properties outlined in the Table 2-3.

The predicted convergence of the unsupported tunnel surface is determined to be 40.7 mm with a plastic zone radius of 8.9 m. if fully grouted bolts (λ = 0.6, diameter 32 mm, and length 6 m) were installed for temporary stabilization of the tunnel, with a bolt density β = 0.08, the extent of the equivalent plastic zone would be reduced by 20 % and the tunnel convergence by 25.3 % approximately. However, a greater bolt density of β = 0.181 would reduce the extent of the plastic zone by 26 % and the tunnel convergence as much as 32 %.

Table 2-4 highlights typical percentage of convergence reduction with respect to the bolt density for a tunnel with the same material properties. It can be appreciably understood that in the case of the excessive yielding , in this case due to the insufficient bolt length (L_b =3 m) in poor rock mass, a high bolt density (β = 0.283) is required to effectively reduce tunnel convergence. In contrast, applying the grouted bolts with enough length (L_b = 6), even more convergence reduction can be achieved in a low bolt density of 0.08. Therefore, it is strongly suggested that in poor rock mass forming a large thickness of plastic zone or in squeezing ground condition, a rock-bolts pattern with appropriate length be installed.

Influence of grouted bolts on tunnel convergence
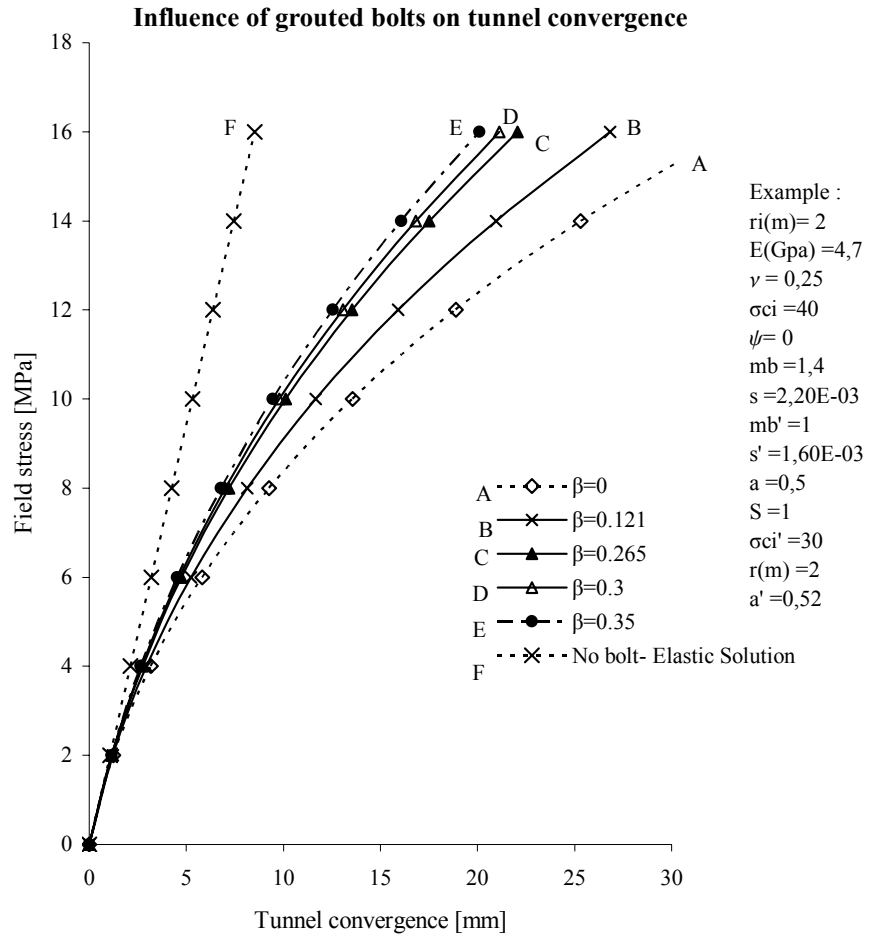
Figure 2-18 Influence of field stress on tunnel convergence for different magnitude of the bolt density parameter

Similarly, Oreste (2003) pointed out it is acceptable to introduce a criterion which prevents the plastic zone radius in the rock mass from exceeding the anchor length of the bolts:

$$r_e^* < (r_i + \ a \cdot L_b) \ , \ \text{where a} = 0.5 - 0.75.$$

Table 2-3 Rock mass properties used in example corresponding to displacement control approach

$E(Gpa)$	2
v	0,25
σ_{ci}	25
ψ	0
mb	0,55
s	2,00E-04
m_b'	0,4
s'	1,70E-04
a	0,531
S	1
σ_{ci}'	20
$r(m)$	3
a'	0,56
$N\psi$	1,0

Table 2-4 The influence of bolt density parameter β on tunnel convergence

L_b (m)	$S_T \cdot S_L$	S_T / L_b	S_L / L_b	β	% Reduction of convergence
		Unsupported		0	0
3	1,5 * 1,5	0,5	0,5	0,08	16
3	1,2 * 1,5	0,4	0,5	0,101	17
3	1,0 * 1,2	0,33	0,4	0,151	18
3	0,8 * 0,8	0,26	0,26	0,283	21
L_b (m)	$S_T \cdot S_L$	S_T / L_b	S_L / L_b	β	% Reduction of convergence
		Unsupported		0	0
6	1,5 * 1,5	0,25	0,25	0,08	25
6	1,2 * 1,5	0,2	0,25	0,101	27
6	1,0 * 1,2	0,16	0,2	0,151	30
6	0,8 * 0,8	0,13	0,13	0,283	40

CONCLUSIONS

Implications on proposed elasto-plastic model

For the elastic–brittle–plastic analysis of circular openings in an infinite Hoek–Brown medium, the existing analytical solutions were found to be very complex and none of them has been developed based on latest Hoek & Brown yields criterion. Therefore, the theoretical analysis presented in this thesis has introduced an alternative elasto-plastic solution to design of grouted bolts for tunnels and to depict the ground reaction curve for both unsupported and reinforced tunnels.

Although most of the existing elasto-plastic solutions for tunnel design in Hoek & Brown media consider an intact rock (i.e., $a = 0.5$), the proposed elasto-plastic solution supposes $a \geq 0.5$ for rock mass. In addition, this solution is based on the assumption that after the intact strength of the rock is exceeded, the material loses its strength, as dictated by a strength loss parameter (S).

The convergence control approach was used for the design of fully grouted bolts. The effectiveness of fully grouted bolts should be assessed on the basis of convergence reduction, which in turn should assist the designer in selecting the optimum reinforcement configuration. The numerical studies have verified the reliability of the analytical solution in the convergence prediction of both un-reinforced and reinforced deep tunnel openings.

The interaction mechanism between rock mass and grouted rock bolts has been based on the Equivalent Strength Parameter such that the global strength of rock mass is increased due to bolts effect. In this approach, the mechanical parameters of rock mass (Hoek & Brown constants m_b, s, and σ_{ci}) are improved through rock bolt density parameter (β).

The influence of the bolt density parameter (β) on the apparent strength of the rock mass profoundly reflects the importance of the bolt spacing and bolt-grout interaction (frictional) in design. In poor rock mass, the use of shaped rebars with a relatively dense bolt configuration is recommended in practice. The evaluation of the Equivalent Plastic Zone radius (r_e^*) as a function of the bolt density parameter and bolt length, provides a fundamental basis for the determination of a reinforced tunnel convergence.

The normalized convergence ratio and the resulting bolt effectiveness are the fundamental design aids introduced in this analysis. The normalized convergence ratio is most appropriate in design, where the strength and frictional parameters are poorly defined.

It can be inferred from the results of analytical study that the installation of an optimum number of grouted bolts immediately on excavation near the tunnel face contributes to a much greater degree of stabilization and the provision of

supplemental bolting at a later stage. It is indeed that initial bolt configuration that is predominant in controlling the extent of overstressing around the tunnel and the final tunnel convergence.

The concept of an Equivalent Plastic Zone was introduced to describe the extent of yielding around a circular tunnel, reinforced with fully grouted bolts. Three stages (categories) of yield propagation have been defined and analyzed with respect to the relative location of the plastic zone boundary in contrast to the neutral point of zero shear stress on the bolt. A friction factor, λ, has been introduced as a characteristic parameter for the bolt-ground composite interaction.

The mathematical treatment of the elasto-plastic analysis has been based on several simplifying assumptions. A circular opening reinforced with an axi-symmetric bolt pattern, excavated in an isotropic, homogeneous medium, subjected to a hydrostatic field stress has been taken into consideration. However, in order to solve the differential equations of incremental plastic strain the use of numerical methods has been adopted. The Equivalent Plastic Zone, as a result, determined by the analytical solution is axi-symmetric or circular in shape. Therefore, the accuracy of the proposed analytical solution becomes questionable as the complexity of the geological conditions and geometry increases.

Since the behaviour of the rock mass is modelled, in this study, by either elastic-perfectly plastic or elastic-brittle-plastic behaviour with a corresponding non-linear Hoek & Brown failure criterion, the rock materials obeying this behaviour are believed to be modelled more accurately and realistically that those analytical solutions based on linear Mohr-Coulomb failure criterion. However, for future study, it is suggested extending this solution to rock material following the strain-softening behaviours.

Since the proposed analytical solution is valid for isotropic medium, it can also be used for fractured and heavy jointed rock mass dominated at least by four sets of discontinuities. Therefore, for rock masses with presence of a considerable discontinuity or fewer than four discontinuities the proposed analytical solution cannot be used.

The influence of time-dependent material properties on ground convergence has not been investigated in this study. Time-dependent loosening can be critical if an opening is left unsupported for a considerable period of time. However, time dependent convergence of a tunnel opening can be minimized by the provision of supports at the face, immediately after excavation. Therefore, it may be deduced that the theoretical convergence predictions are realistic, if fully grouted bolts are installed soon after excavation. In this respect, the primary NATM design objective is also acknowledged.

The rational approach for the design of fully grouted bolts for underground excavations in yielding rock presented in this thesis clearly illustrates the capability of the fully grouted bolts in controlling rock mass displacements.

Implications on the advancing tunnel face

The proposed analytical solution predicts the ultimate convergence (more than two tunnel diameter behind the face). 3-D effects close to the face have been neglected. Therefore, the convergence ratio and the bolt effectiveness introduced in this analysis are related to a 2-D solution. In reality, the observed convergence (u_r) is affected by the face effects, and is generally less than the predicted total convergence (u_t) by the amount of displacement (u_i) which occurs ahead of the face or prior to initial measurement.

Panet & Guenot (1982) have presented numerical analyses of the advancing face effect (k=1) for circular tunnels driven through elasto-plastic material. In their solutions, the prediction of the convergence profile behind the face requires a preliminary assessment of the ultimate time-independent closure and the final extent of the plastic zone. The final convergence of the numerical axi-symmetric model of the tunnel, whose properties outlined in Table 1-2, has been quite close to result of proposed analytical solution. As can be seen from Figure 1-19 the displacement at tunnel face is 30 % of final displacement. Alternatively, several in-situ convergence measurements behind the face may be utilized for the purpose of semi-empirical solution. However, the ultimate convergence and the corresponding plastic zone radius for both unsupported and reinforced openings can be determined by the analytical solution proposed in this thesis. Consequently, the 3-D convergence response near the tunnel face may be extrapolated from the ultimate time-independent behaviour.

REFERENCES

1. Barton N, Lien R, Lunde J. 1974. Engineering classification of rock masses for the design of tunnel support. Rock Mechanics; 6(4):189–239.

2. Bieniawski, Z.T., 1973. Engineering classification of jointed rock masses. Trans. S. Afr. Inst. Civ. Eng. 15, 335 344.

3. Bieniawski, Z. T. 1976. Rock mass classification of jointed rock masses. In Exploration for Rock Engineering (Z. T. Bieniawski, ed.), 97-106. Johannesburg: A.A. BaIkema.

4. Brown, E. T., Bray. J. W., Landanyi. B. and Hoek. E. 1983. Ground response curves for rock tunnels. J. Geothechnical Engng .109, 15-39.

5. Carranza-Torres, C. & Fairhurst, C. 1999. The elasto-plastic response of underground excavations in rock masses that satisfy the Hoek-Brown failure criterion. International Journal of Rock Mechanics and Mining Sciences 366, 777–809.

6. Carranza-Torres, C. & Fairhurst, C. 2000. Application of the convergence-confinement method of tunnel design to rock masses that satisfy the Hoek-Brown failure criterion. Tunnelling and Underground Space technology, Vol. 15, No2,pp 187-213.

7. Carranza-Torres, C. 2004. Elasto-plastic solution of tunnel problems using the generalized form of the Hoek-Brown failure criterion. International Journal of Rock Mechanics and Mining Sciences. 41supplement 1, 629-639.

8. Cundall, P., Carranza-Torres, C. & Hart, R. 2003. A new constitutive model based on the hoek-brown failure criterion. In Itasca Consulting Group Inc. Ed., Proceedings of the Third International FLAC Symposium. "FLAC and Numerical Modelling in Geomechanics", Sudbury, Canada. October 21 to 24, 2003. Balkema.

9. Detournay, E & John, C. M. 1988. Design charts for a deep circular tunnel under non-uniform loading. Rock Mechanics and Rock Engineering. 21, 119-137.

10. Ducan Fama, M. E. 1993. Numerical modelling of yield zones in weak rocks. In Comprehensive rock engineering, (ed. J.A. Hudson) **2**, 49-75. Oxford: Pergamon.

11. Florence, A. L & Schwer, L. E. 1978. Axisymmetric compression of a Mohr-Coulomb medium around a circular hole. Int. J. Numer. Anal. Meth. Geomech. 2, pp, 367-379.

12. Freeman. T. J. 1978. The behaviour of fully-bonded rock bolts in the Kielder experimental tunnel. Tunnels & Tunnelling 10. pp.37-40.

13. Fritz, P. 1984. An analytical solution for axisymmetric tunnel problems in elasto-viscoplastic media. Int. J. Numer. Anal. Meth. Geomech.. 8, pp, 325-342.

14. Grasso, P., Mahtab, A., Pelizza, S., 1989. Riqualificazione della massa rocciosa: un criterio per la stabilizzazione delle gallerie. Gallerie Grandi Opere Sotterranee 29, 35–41.

15. Graziani A. e Ribacchi R. 1993. Stato di Sforzo e di Deformazione intorno ad una Galleria sostenuta con Barre Passive, Atti XVIII Convegno Nazionale di Geotecnica, Rimini, AGI, pp.213-227

16. Hill, R. 1950. The mathematical theory of plasticity. Oxford Science Publications.

17. Hoek, E. and Brown, E.T. 1980a. Empirical strength criterion for rock masses. J. Geotech. Engng Div., ASCE 106(GT9), 1013-1035.

18. Hoek E. and Brown E.T. 1980b. Underground Excavations in Rock. London: Institution of Mining and Metallurgy 527 pages.

19. Hoek, E. 1994. Strength of rock and rock masses, ISRM News Journal, 2(2), 4-16.

20. Hoek, E., Kaiser, P.K. and Bawden, W.F. 1995. Support of underground excavation in hard rock, A. A. Balkema.

21. Hoek, E. and E.T. Brown. 1997. Practical estimates of rock mass strength. Int J Rock Mech Min Sci; 34(8), 1165-1186.

22. Hoek, E., Marinos, P. and Benissi, M. 1998 Applicability of the Geological Strength Index (GSI) classification for very weak and sheared rock masses. The case of the Athens Schist Formation. Bull. Engg. Geol. Env. 57(2), 151-160.

23. Hoek, E. and Marinos, P. 2000. Predicting Tunnel Squeezing. Tunnels and Tunnelling International. Part 1 - November Issue. 45-51, Part 2 - December, 34-36.

24. Hoek, E. 2001. Big tunnels in bad rock. The Thirty-Sixth Karl Terzaghi Lecture. Journal of Geotechnical and Geoenvironmental Engineering. Vol. 127. pp. 726-740.

25. Hoek E, Carranza-Torres CT, Corkum B. 2002. Hoek-Brown failure criterion-2002 edition. In: Proceedings of the Fifth North American Rock Mechanics Symposium, Toronto, Canada, Vol. 1,. p. 267–73.

26. Indraratna, B.1987. Application of fully grouted bolts in yielding rock. Ph.D thesis, University of Alberta.

27. Indraratna, B. & Kaiser. P. K.1987.Wall convergence in tunnels supported by fully grouted bolts. 28th U.S.Symp.on Rock Mech., Tuscon, Arizona, pp.843-852.

28. Indraratna, B. & Kaiser, P. K. 1990a.Analytical model for the design of grouted rock bolts. International Journal for Numerical and Analytical Methods in Geomechanics. Vol 14. No.4, 227-251.

29. Indraratna, B. & Kaiser. P. K. 1990b. Design for grouted rock bolts based on the convergence control method. Int. J. Rock mech. Mining Sci. & Geomech. Abstr. 27, 269-281.

30. Itasca Consulting Group, Inc. 2000. FLAC (Fast Lagrangian Analysis of Continua) Version 4.0. www.itascacg.com , Minneapolis.

31. John, C. M., Detournay, E. Fairhurst, C. 1984. Design charts for a deep circular tunnel under non-hydrostatic loading. 25th Symposium on rock mechanics in rock mechanics in productivity and production. pp 849-856.

32. Ladanyi, B. Use of long-term strength concept in the determination of ground pressure on tunnel linings. Proc. 3rd Congr., Intnl. Soc. Rock Mech., Denver, 1974, Vol 2B, pp 1150-1156.

33. Maple V 9. 2003. Waterloo Maple Inc.

34. Mathematica V 5.1. 2004. Wolfram Research.

35. Michelis, P & Brown, E, T. 1986. A yield equation for rock. Canadian Geotechnical Journal. 23, 9-17.

36. Ogawa, T & Lo, K. Y. 1987. Effect of dilatancy and yield criteria on displacement around tunnels. Can. Geotech. J. 24, 100-113.

37. Oreste, P. P. & Peila, D. 1996. Radial passive rockbolting in tunnelling design with a new convergence- confinement model. Int. J. Rock mech. Mining Sci. & Geomech. Abstr. 33, 443-454.

38. Oreste, P. P. 2002. Il metodo convergenza-cofinamento: ruolo e limiti nella moderna progettazione geotecnica delle gallerie, Gallerie e grandi opere sotterranee, vol. 66, April, pp. 34–50.

39. Oreste. P. P. 2003. Analysis of structural interaction in tunnels using the covergence–confinement approach. Tunnelling and Underground Space technology, Vol. 18. pp 347-363.

40. Osgoui, R. 2006. Development of an Elasto-Plastic Model to Design of Grouted Rock-bolts for Tunnels with Particular Reference to Poor Rock Mass. Ph. D thesis. Middle East Technical University. Ankara. 213 pages.

41. Pan, Y. W & Chen, Y. M. 1990. Plastic zones and characteristics-line families for openings in elasto-plastic rock mass. Rock Mechanics and Rock Engineering. 23. pp 275-292.

42. Panet, M & Guenot, A. 1982. Analysis of convergence behind the face of a tunnel. Proc. Tunnelling' 82. pp 197-204. Brighton.

43. Panet, M. 1993. Understanding deformations in tunnels. In Comprehensive rock engineering, (ed. J.A. Hudson) **1**, 663-690. Oxford: Pergamon.

44. Park, K, H & Kim, Y, J. 2006. Analytical solution for a circular opening in an elastic–brittle–plastic rock. Int J Rock Mech Min Sci; 43, 616-622.

45. Peila, I. D & Oreste, P. P.1995. Axisymmetric analysis on ground reinforcing in tunnelling design. Computers and Geotechnics. Vol 17. 253-274.

46. Peila. D., Oreste. P. P., Pelizza. S. 1997. Influence of face plate behaviour on bolt support action. Int. Symp on Rock Support applied solutions for underground structures, Lillehammer, Norway.pp 296-306.

47. Pelizza, S., Kim, S. and Kim, J. 2006. A Study of Strength Parameters in the Reinforced Ground by Rock Bolts. Proceedings of the World Tunnel Congress and 32nd ITA Assembly, Seoul, Korea. pita 06-0385.

48. Press, W. H., Flannery, B. P., Teukolsky, S. A. & Vetterling, W. T. 1994. Numerical Recipies in C. The art of scientific computing (Second ed.). New York: Cambridge University Press.

49. Rocscience, 1999. A 2-D finite element program for calculating stresses and estimating support around the underground excavations. Geomechanics Software and Research, Rocscience Inc., www.rocscience.com Toronto, Ontario, Canada.

50. Senseny, P. E., Lindberg, H. E., Schwer, L. E. 1989. Elastic-plastic response of a circular hole to repeated loading. . Int. J. Numer. Anal. Meth. Geomech.. 13, pp, 459-476.

51. Sharan, S. K. 2003. Elastic-brittle-plastic analysis of circular openings in Hoek-Brown media. Int J Rock Mech Min Sci; 40:817-824.

52. Sharan, S. K. 2005. Exact and approximate solutions for displacements around circular openings in elastic–brittle–plastic Hoek–Brown rock. Int J Rock Mech Min Sci; 42:542–549.

53. Timoshenko, S. P. and Goodier, J. N. 1970. Theory of Elasticity. 3rd Edition. McGraw Hill, New York.

54. Wang, Y. 1996. Ground response of a circular tunnel in poorly consolidated rock. ASCE J. Geotech. Eng. 1229, 703–708.

55. Ward. W. H., Tedd. P.and Berry. N. S. M. 1983. The Kielder experimental tunnel: final results. Géotechnique 33, No. 3, pp. 275-291.

56. Xueyi, S. 1983. Grouted rock bolt used in underground engineering in soft surrounding rock or in highly stressed regions. Proceedings of the International symposium on Rock Bolting. Edited by: O.Stephansson, Abisko, Sweden .pp93-99.

57. Yu, T. Z & Xian, C. J. 1983.Behaviour of rock bolting as tunnelling support. Proceedings of the International symposium on Rock Bolting. Edited by: O.Stephansson, Abisko, Sweden.pp 87-92.

APPENDIX A

NUMERICAL INTEGRATION METHOD USED IN ELASTO-PLASTIC SOLUTION

In order to evaluate the integration stems from the solution of the differential equation of plastic strain (Equation 5-46), the use of one of numerical solutions has been realized to be rational. The Simpsom's rule is chosen to solve the integration approximately. The integration which must be solved numerically is:

$$\left[\int_{r}^{r_e} r^{N_\psi - 1}\left[s'^{1-a'} + m_b'(1-a')\ln\left(\frac{r}{r_i}\right)\right]^{\frac{a'}{1-a'}} dr\right] \tag{A-1}$$

The Fundamental Theorem of Calculus gives us an exact formula for computing $\int_a^b f(x)\,dx$, provided we can find an antiderivative for f. This method of evaluating definite integrals is called the **analytic** method. However, there are times when this is difficult or impossible. In these cases, it is usually good enough to find an approximate or **numerical** solution, and there are some very straightforward ways to do this.

The simplest numerical approximations to the integral are the **left and right Riemann sums.** More efficient approximations are the **trapezoidal** and **Simpson** approximations.

Simpson's rule is a **Newton-Cotes** formula for approximating the integral of a function *f* using quadratic polynomials (i.e., parabolic arcs instead of the straight line segments used in the trapezoidal rule). Simpson's rule can be derived by integrating a third-order Lagrange interpolating polynomial fit to the function at three equally spaced points. We start by partitioning [a, b] into intervals all of the same width, but this time we must use an even number of intervals, so n will be even. In particular, let the function *f* be tabulated at points x_0, x_1, and x_2 equally spaced by distance $\frac{(b-a)}{n}$, and denote $f_n = f(x_n)$. Then Simpson's rule states that if n is even then

$$x_k = a + k\Delta x = a + k\frac{(b-a)}{n} \tag{A- 2}$$

$$\int_a^b f(x)dx \approx \frac{b-a}{3n}\begin{bmatrix} f(x_0) + 4f(x_1) + 2f(x_2) + 4f(x_3) + \\ ... + 2f(x_{n-2}) + 4f(x_{n-1}) + f(x_n) \end{bmatrix} \tag{A- 3}$$
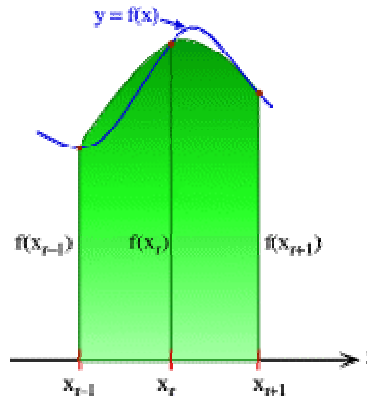
Figure A-0-1 The function $f(x)$ (in blue) is approximated by a quadratic function $P(x)$ (in green).

As with the trapezoid rule, we want to approximate the areas in each strip by something more complicated than a rectangle. This time we take the strips in pairs (which is why we need an even number of them) and draw a parabola through the three points $(x_{k-1}, f(x_{k-1}))$, $(x_k, f(x_k))$, and $(x_{k+1}, f(x_{k+1}))$, as shown in the Figure A-0-1. It is then not too difficult to find the equation of this parabola (it has the form $y = Ax^2 + Bx + C$), and from that to find the area underneath by integrating. The remarkably simple answer is:

$$\textbf{Area under parabola } \textit{P (x)} = \frac{b-a}{3n}\left[f(x_{k-1}) + 4f(x_k) + f(x_{k+1})\right] \tag{A- 4}$$

When we add the area under the parabola over the first two strips to the area under the parabola over the 3rd and 4th strips, and so on, we get Simpson's rule.

Considering the parameters included in Table 1-2, the approximate result of the integration A-1 used in elasto-plastic solution will be 0.84451.

APPENDIX B

SPREADSHEET IMPLEMENTATION OF THE PROPOSED ANALYTICAL SOLUTION

Elastic-Brittle-Plastic analysis for circular tunnels in Hoek & Brown media [undertaken in Torino 27 06 2006]				Middle East Technical University		Politecnico di Torino	
Input and Output							
ri(m)	2		**Stresses analysis**				
Po (MPa)	15		**Stress in plastic zone**		**Strains and displacements Analysis**		
E(Gpa)	5.7		G(Mpa)	2192.30769	**Strains in elastic zone**		
ν	0.3		k(Mpa)	4750	εr	-1.05E-02	
σci	30				ε?	1.32E-02	
ψ	0		σ? (MPa)	1.30766968			
mb	1.7		M	2.96E-01			
s	3.90E-03		σre(MPa)	6.12E+00			
mb'	0.85				**Strains in plastic zone**		
s'	1.90E-03		Ω	0.057	elastic	εre	-8.95E-05
a	0.5		σr(MPa)	0.0000	strains	ε?e	2.09E-04
S	1		re(m)	4.83361934			
σci'	30						Brown BC
r(m)	2				plastic	ε?p	1.40E-02
a'	0.5		**Stress in elastic zone**		strains	εrp	
Nψ	1.0		σ? (MPa)	66.8779697			
λ(integrand)	0.73202		σr(MPa)	-36.8779697		εrt	-8.95E-05
Pi(Mpa)	0.00				total strains	ε?t	1.42E-02
γ(MN/m3)	2.40E-02						
Maximum radial distance (to plot results)							
Rmax [m]:	10		(Rmax)				
Grouted Rock bolt Effect							
λ	0.6	β	0.121				
d (mm)	32.00	mb*	0.953				
Cb (kN)	280.00	σci*	33.619				
St (m)	1.00	s*	2.129E-03				
Sl (m)	1.00						
Lb (m)	3.00	mb1	0.747				
ρ(m)	3.27	σci1	26.381				
		s1	1.671E-03				

Unsupported Tunnel case						
Boundary conditions						
ur1 [m]:	0.00979127					
ur1P [m]:	0.0098					
Solution for the elastic region						
point	r [m]	rho	sigr [MPa]	sigt [MPa]	ur [m]	
1	10.0000	2.069	12.9249	17.0751	0.0047	
2	9.7281	2.013	12.8073	17.1927	0.0049	
3	9.4562	1.956	12.6793	17.3207	0.0050	
4	9.1843	1.900	12.5399	17.4601	0.0052	
5	8.9123	1.844	12.3875	17.6125	0.0053	
6	8.6404	1.788	12.2205	17.7795	0.0055	
7	8.3685	1.731	12.0369	17.9631	0.0057	
8	8.0966	1.675	11.8345	18.1655	0.0058	
9	7.8247	1.619	11.6107	18.3893	0.0060	
10	7.5528	1.563	11.3623	18.6377	0.0063	
11	7.2809	1.506	11.0855	18.9145	0.0065	
12	7.0089	1.450	10.7759	19.2241	0.0068	
13	6.7370	1.394	10.4280	19.5720	0.0070	
14	6.4651	1.338	10.0353	19.9647	0.0073	
15	6.1932	1.281	9.5898	20.4102	0.0076	
16	5.9213	1.225	9.0815	20.9185	0.0080	
17	5.6494	1.169	8.4980	21.5020	0.0084	
18	5.3774	1.113	7.8239	22.1761	0.0088	
19	5.1055	1.056	7.0391	22.9609	0.0093	
20	4.8336	1.000	6.1183	23.8817	0.0098	
(pt_E)	(r_E)	(rho_E)	(sigr_E)	(sigt_E)	(ur_E)	
Solution for the plastic region						
point	r [m]	rho	sigr [MPa]	sigt [MPa]	Ω	λ(integrand)	ur [m]
1	4.8336	1.0000	6.1183	18.6771	5.2575	0.0000	0.0098
2	4.6845	0.9691	5.7309	17.8902	4.9283	0.0614	0.0103
3	4.5353	0.9383	5.3442	17.0910	4.5996	0.1209	0.0107
4	4.3862	0.9074	4.9585	16.2790	4.2718	0.1782	0.0113
5	4.2371	0.8766	4.5746	15.4540	3.9454	0.2334	0.0118
6	4.0879	0.8457	4.1929	14.6154	3.6210	0.2864	0.0124
7	3.9388	0.8149	3.8144	13.7631	3.2992	0.3370	0.0130
8	3.7897	0.7840	3.4399	12.8964	2.9809	0.3852	0.0137
9	3.6405	0.7532	3.0705	12.0151	2.6669	0.4310	0.0144
10	3.4914	0.7223	2.7075	11.1188	2.3583	0.4741	0.0151
11	3.3422	0.6915	2.3524	10.2071	2.0566	0.5146	0.0159
12	3.1931	0.6606	2.0071	9.2799	1.7631	0.5522	0.0168
13	3.0440	0.6297	1.6739	8.3367	1.4798	0.5868	0.0178
14	2.8948	0.5989	1.3552	7.3776	1.2090	0.6184	0.0188
15	2.7457	0.5680	1.0545	6.4025	0.9534	0.6467	0.0200
16	2.5966	0.5372	0.7757	5.4116	0.7164	0.6715	0.0212
17	2.4474	0.5063	0.5238	4.4055	0.5023	0.6927	0.0226
18	2.2983	0.4755	0.3050	3.3850	0.3162	0.7100	0.0242
19	2.1491	0.4446	0.1270	2.3517	0.1650	0.7232	0.0259
20	2.0000	0.4138	0.0000	1.3077	0.0570	0.7320	0.0279
(pt_P)	(r_P)	(rho_P)	(sigr_P)	(sigt_P)	(c_k1)		(ur_P)

Grouted Bolts Effect Min.Yielding						
Boundary conditions						
ur1 [m]:	0.008861415					
ur1P [m]:	0.0089					
Solution for the elastic region						
point	r [m]	rho	sigr [MPa]	sigt [MPa]	ur [m]	
1	10.0000	2.286	13.3003	16.6997	0.0039	
2	9.7039	2.218	13.1950	16.8050	0.0040	
3	9.4079	2.151	13.0796	16.9204	0.0041	
4	9.1118	2.083	12.9528	17.0472	0.0043	
5	8.8157	2.015	12.8130	17.1870	0.0044	
6	8.5196	1.948	12.6583	17.3417	0.0046	
7	8.2236	1.880	12.4867	17.5133	0.0047	
8	7.9275	1.812	12.2954	17.7046	0.0049	
9	7.6314	1.744	12.0815	17.9185	0.0051	
10	7.3353	1.677	11.8411	18.1589	0.0053	
11	7.0393	1.609	11.5698	18.4302	0.0055	
12	6.7432	1.541	11.2620	18.7380	0.0057	
13	6.4471	1.474	10.9108	19.0892	0.0060	
14	6.1510	1.406	10.5076	19.4924	0.0063	
15	5.8550	1.338	10.0418	19.9582	0.0066	
16	5.5589	1.271	9.4996	20.5004	0.0070	
17	5.2628	1.203	8.8633	21.1367	0.0074	
18	4.9667	1.135	8.1098	21.8902	0.0078	
19	4.6707	1.068	7.2086	22.7914	0.0083	
20	4.3746	1.000	6.1183	23.8817	0.0089	
(pt_E)	(r_E)	(rho_E)	(sigr_E)	(sigt_E)	(ur_E)	
Solution for the plastic region						
point	r [m]	rho	sigr [MPa]	sigt [MPa]	Ω	λ(integrand)	ur [m]
1	4.3746	1.0000	6.1183	18.6771	5.8995	0.0000	0.0089
2	4.2496	0.9714	5.7168	17.8612	5.5171	0.0463	0.0092
3	4.1246	0.9429	5.3174	17.0350	5.1366	0.0909	0.0097
4	3.9996	0.9143	4.9206	16.1983	4.7587	0.1340	0.0101
5	3.8747	0.8857	4.5272	15.3509	4.3839	0.1754	0.0105
6	3.7497	0.8572	4.1377	14.4925	4.0129	0.2152	0.0110
7	3.6247	0.8286	3.7532	13.6232	3.6467	0.2531	0.0115
8	3.4997	0.8000	3.3745	12.7426	3.2860	0.2892	0.0120
9	3.3748	0.7714	3.0029	11.8508	2.9320	0.3234	0.0126
10	3.2498	0.7429	2.6397	10.9476	2.5860	0.3556	0.0132
11	3.1248	0.7143	2.2863	10.0330	2.2494	0.3858	0.0138
12	2.9998	0.6857	1.9447	9.1071	1.9240	0.4139	0.0145
13	2.8748	0.6572	1.6170	8.1700	1.6118	0.4398	0.0153
14	2.7499	0.6286	1.3056	7.2219	1.3152	0.4633	0.0161
15	2.6249	0.6000	1.0136	6.2631	1.0371	0.4845	0.0169
16	2.4999	0.5715	0.7446	5.2941	0.7809	0.5031	0.0178
17	2.3749	0.5429	0.5029	4.3153	0.5506	0.5190	0.0189
18	2.2500	0.5143	0.2937	3.3268	0.3514	0.5322	0.0200
19	2.1250	0.4858	0.1234	2.3275	0.1892	0.5424	0.0212
20	2.0000	0.4572	0.0000	1.3077	0.0716	0.5494	0.0226
(pt_P)	(r_P)	(rho_P)	(sigr_P)	(sigt_P)	(c_k1)		(ur_P)

Grouted Bolts Effect Major.Yielding						
Boundary conditions						
ur1 [m]:	0.009601653					
ur1P [m]:	0.0096					
Solution for the elastic region						
point	r [m]	rho	sigr [MPa]	sigt [MPa]	ur [m]	
1	10.0000	2.110	13.0045	16.9955	0.0046	
2	9.7232	2.051	12.8892	17.1108	0.0047	
3	9.4463	1.993	12.7637	17.2363	0.0048	
4	9.1695	1.934	12.6266	17.3734	0.0050	
5	8.8926	1.876	12.4765	17.5235	0.0051	
6	8.6158	1.818	12.3118	17.6882	0.0053	
7	8.3390	1.759	12.1303	17.8697	0.0055	
8	8.0621	1.701	11.9299	18.0701	0.0056	
9	7.7853	1.642	11.7076	18.2924	0.0058	
10	7.5084	1.584	11.4604	18.5396	0.0061	
11	7.2316	1.526	11.1842	18.8158	0.0063	
12	6.9547	1.467	10.8743	19.1257	0.0065	
13	6.6779	1.409	10.5252	19.4748	0.0068	
14	6.4011	1.350	10.1297	19.8703	0.0071	
15	6.1242	1.292	9.6795	20.3205	0.0074	
16	5.8474	1.234	9.1637	20.8363	0.0078	
17	5.5705	1.175	8.5692	21.4308	0.0082	
18	5.2937	1.117	7.8790	22.1210	0.0086	
19	5.0169	1.058	7.0714	22.9286	0.0091	
20	4.7400	1.000	6.1183	23.8817	0.0096	
(pt_E)	(r_E)	(rho_E)	(sigr_E)	(sigt_E)	(ur_E)	
Solution for the plastic region						
point	r [m]	rho	sigr [MPa]	sigt [MPa]	Ω	λ(integrand)	ur [m]
1	4.7400	1.0000	6.1183	18.6771	5.8995	0.0000	0.0096
2	4.5958	0.9696	5.7168	17.8612	5.5171	0.0582	0.0101
3	4.4516	0.9392	5.3174	17.0350	5.1366	0.1145	0.0105
4	4.3074	0.9087	4.9206	16.1983	4.7587	0.1689	0.0110
5	4.1632	0.8783	4.5272	15.3509	4.3839	0.2211	0.0115
6	4.0190	0.8479	4.1377	14.4925	4.0129	0.2713	0.0121
7	3.8747	0.8175	3.7532	13.6232	3.6467	0.3192	0.0127
8	3.7305	0.7870	3.3745	12.7426	3.2860	0.3649	0.0133
9	3.5863	0.7566	3.0029	11.8508	2.9320	0.4082	0.0140
10	3.4421	0.7262	2.6397	10.9476	2.5860	0.4490	0.0147
11	3.2979	0.6958	2.2863	10.0330	2.2494	0.4873	0.0155
12	3.1537	0.6653	1.9447	9.1071	1.9240	0.5228	0.0164
13	3.0095	0.6349	1.6170	8.1700	1.6118	0.5556	0.0173
14	2.8653	0.6045	1.3056	7.2219	1.3152	0.5855	0.0183
15	2.7211	0.5741	1.0136	6.2631	1.0371	0.6122	0.0193
16	2.5768	0.5436	0.7446	5.2941	0.7809	0.6357	0.0205
17	2.4326	0.5132	0.5029	4.3153	0.5506	0.6558	0.0218
18	2.2884	0.4828	0.2937	3.3268	0.3514	0.6722	0.0233
19	2.1442	0.4524	0.1234	2.3275	0.1892	0.6848	0.0249
20	2.0000	0.4219	0.0000	1.3077	0.0716	0.6932	0.0268
(pt_P)	(r_P)	(rho_P)	(sigr_P)	(sigt_P)	(c_k1)		(ur_P)

Grouted Bolts Effect Exceeding.Yielding						
Boundary conditions						
ur1 [m]:	0.009663988					
ur1P [m]:	0.0100					
Solution for the elastic region						
point	r [m]	rho	sigr [MPa]	sigt [MPa]	ur [m]	
1	10.0000	2.096	12.9785	17.0215	0.0046	
2	9.7248	2.038	12.8624	17.1376	0.0047	
3	9.4496	1.981	12.7361	17.2639	0.0049	
4	9.1743	1.923	12.5982	17.4018	0.0050	
5	8.8991	1.865	12.4474	17.5526	0.0052	
6	8.6239	1.808	12.2819	17.7181	0.0053	
7	8.3487	1.750	12.0997	17.9003	0.0055	
8	8.0734	1.692	11.8986	18.1014	0.0057	
9	7.7982	1.635	11.6758	18.3242	0.0059	
10	7.5230	1.577	11.4281	18.5719	0.0061	
11	7.2478	1.519	11.1517	18.8483	0.0064	
12	6.9726	1.462	10.8419	19.1581	0.0066	
13	6.6973	1.404	10.4931	19.5069	0.0069	
14	6.4221	1.346	10.0986	19.9014	0.0072	
15	6.1469	1.288	9.6498	20.3502	0.0075	
16	5.8717	1.231	9.1365	20.8635	0.0079	
17	5.5965	1.173	8.5457	21.4543	0.0082	
18	5.3212	1.115	7.8607	22.1393	0.0087	
19	5.0460	1.058	7.0607	22.9393	0.0091	
20	4.7708	1.000	6.1183	23.8817	0.0097	
(pt_E)	(r_E)	(rho_E)	(sigr_E)	(sigt_E)	(ur_E)	
Solution for the plastic region						
point	r [m]	rho	sigr [MPa]	sigt [MPa]	Ω	λ(integrand)	ur [m]
1	4.7708	1.0000	6.1183	18.6771	5.8995	0.1565	0.0100
2	4.6250	0.9694	5.7168	17.8612	5.5171	0.2027	0.0105
3	4.4791	0.9389	5.3174	17.0350	5.1366	0.2474	0.0109
4	4.3333	0.9083	4.9206	16.1983	4.7587	0.2905	0.0114
5	4.1875	0.8777	4.5272	15.3509	4.3839	0.3319	0.0119
6	4.0416	0.8472	4.1377	14.4925	4.0129	0.3716	0.0125
7	3.8958	0.8166	3.7532	13.6232	3.6467	0.4096	0.0131
8	3.7500	0.7860	3.3745	12.7426	3.2860	0.4457	0.0137
9	3.6041	0.7555	3.0029	11.8508	2.9320	0.4799	0.0143
10	3.4583	0.7249	2.6397	10.9476	2.5860	0.5121	0.0151
11	3.3125	0.6943	2.2863	10.0330	2.2494	0.5423	0.0158
12	3.1666	0.6638	1.9447	9.1071	1.9240	0.5704	0.0167
13	3.0208	0.6332	1.6170	8.1700	1.6118	0.5962	0.0176
14	2.8750	0.6026	1.3056	7.2219	1.3152	0.6198	0.0185
15	2.7292	0.5721	1.0136	6.2631	1.0371	0.6409	0.0196
16	2.5833	0.5415	0.7446	5.2941	0.7809	0.6595	0.0208
17	2.4375	0.5109	0.5029	4.3153	0.5506	0.6755	0.0221
18	2.2917	0.4804	0.2937	3.3268	0.3514	0.6886	0.0236
19	2.1458	0.4498	0.1234	2.3275	0.1892	0.6988	0.0253
20	2.0000	0.4192	0.0000	1.3077	0.0716	0.7059	0.0272
(pt_P)	(r_P)	(rho_P)	(sigr_P)	(sigt_P)	(c_k1)		(ur_P)

			Pi Effect	
Case I. re*<ρ< (a+L) minimal yielding				
			Pi Effect	
	Y	0.783	**0.783**	
	re*	4.375	**4.375**	
Case II. ρ<re*< (a+L) major yielding				
	Γ*		0.079	
	σρ		2.710	
	h		0.493	
	J		0.370	
	re*		4.740	
Case III. re*>(a+L) excessive yielding				
	Γ*	0.079		
	σρ	2.710		
	h	0.493		
	ξ	5.068		
	σL	6.722		
	t	0.423		
	q	-0.047		
	re*	4.771		

Minimal yielding
$r_e^* < ? < (r_i + L_b)$

Major yielding
$? < r_e^* < (r_i + L_b)$

Excessive yielding
$r_e^* > (r_i + L_b)$